NBSIR 86-3322

A Vortex-Induced, Gas-Liquid Separation in a Cylindrical Tank at Zero Gravity

T.T. Yeh

U.S. DEPARTMENT OF COMMERCE
National Bureau of Standards
Center for Chemical Engineering
Gaithersburg, MD 20899

February 1986

Prepared for:

National Aeronautics and Space Administration
John F. Kennedy Space Center
Kennedy Space Center, FL 32899

NBSIR 86-3322

A VORTEX-INDUCED, GAS-LIQUID SEPARATION IN A CYLINDRICAL TANK AT ZERO GRAVITY

T. T. Yeh

U.S. DEPARTMENT OF COMMERCE
National Bureau of Standards
Center for Chemical Engineering
Gaithersburg, MD 20899

February 1986

Prepared for:

National Aeronautics and Space Administration
John F. Kennedy Space Center
Kennedy Space Center, FL 32899

U.S. DEPARTMENT OF COMMERCE, Malcolm Baldrige, *Secretary*
NATIONAL BUREAU OF STANDARDS, Ernest Ambler, *Director*

Table of Contents

ABSTRACT

The absence of body force and the natural orientations of two phase-gas-liquid systems in space produce major differences between liquid fuel transfer in space and that on earth. A vortex-induced, liquid handling process adapted to two-phase fluids in zero gravity has been analyzed for a selected range of fluid and flow parameters. This transfer process has been divided in two stages: the initial "spin-up" stage and the liquid "pump-out" stage from the "sender" tank. The initial spin-up stage is established by tangential fluid injection. The model is based on a two-phase, two-fluid continuum with several phase interactions - namely fluid drag and pertinent virtual mass effects.

A computer program was developed to study the fluid dynamical behavior of two-phase fluids in the sender tank. Several examples are given to demonstrate the products of the program. The interesting and plausible results indicate the simplified two-phase, two-fluid model is a very useful one. However, detailed evaluations of the results are only possible with accurate local measurements. These verifications should be devised and carried out to check both the formulations selected for phase interactions as well as the results predicted.

Key Words: Fuel transfer in zero gravity, gas-liquid separation, numerical modeling, rotational flows, two-phase flows, vortex motions, vortex-induced phase separations.

List of Notations

A_a, A_{ak}	Added mass coefficients
A_d, A_{dk}	Drag coefficients
$\bar{B}_k$	Body force density
C_{ij}, C_{pk}, C_{dk}	Generalized coefficients defined in Eq. (20)
$\bar{\bar{D}}$	$1/2\ (\nabla\bar{V} + \bar{V}\nabla)$, deformation tensor
d_1	Bubble diameter
d_2	Liquid (droplet) diameter
H_j	Effective injection region
h	Jet penetration depth
$\bar{\bar{I}}$	Unit tensor
I_w	Boundary condition. I_w = 1 non-slip, = 0 free surface.
M_a	Angular momentum
$\bar{M}_k$	Effective interfacial force density
MXI	$\overline{\alpha_1\alpha_2}/\bar{\alpha}_1\bar{\alpha}_2$, mixing index
n	Regular time step
$\bar{n}$	Unit vector
n_a	Exponent used for w_{ak}
n_d	Exponent used for w_{dk}
p	Pressure

Q_j	Jet volume flow rate
$\bar{Q}_r$	Separation strength
q_j	Jet volume flow rate density
R	Tank radius
R_c	Interfacial radius between core vapor and annual liquid when they are separated completely
Re	$\rho_2 V_s R/\mu_2$, Reynolds number
R_{j1}, R_{j2}	Jet opening, $R_{j1} < r < R_{j2}$
R_1	Minimum radius considered in the numerical analysis
$\bar{R}_k$	The center of gravity
$\bar{R}_{km}$	Value of $\bar{R}_k$ when two phases are completely separated
r	Radial coordinate
SPI	Separation index
$\bar{\bar{T}}$	$-p\bar{\bar{I}} + \bar{\bar{\tau}}$ total stress tensor
t	Time
t*	Time at which the pump-out stage is started
t**	Time at which the pump-out stage is stopped
V_j	Averaged jet velocity
V_{r1}	Gas radial velocity
V_{r2}	Liquid radial velocity
V_s	Velocity scale

$V_{\theta 1}$	Gas tangential velocity
$V_{\theta 2}$	Liquid tangential velocity
$\bar{V}_1$	Gas velocity
$\bar{V}_2$	Liquid velocity
w_{ak}	Weighting function for added mass coefficients
w_{dk}	Weighting function for drag coefficients
α_1	Gas volume fraction
α_2	$(1-\alpha_1)$, liquid volume fraction
$\bar{\alpha}_2(r_1,r_2)$	$2\int_{r_1}^{r_2} \alpha_2\, rdr/(r_2^2-r_1^2)$, liquid purity
Γ	Vortex strength
γ	Exponent for diameter variation
κ	Curvature of local interfacial surface
θ	Circumferential coordinate
μ_1	Gas dynamic viscosity
μ_2	Liquid dynamic viscosity
μ_k^e	$\mu_k + \mu_k^t$ total effective viscosity
μ_k^t	Turbulence or eddy viscosity
ν_k	μ_k/ρ_k, kinematic viscosity
ρ_1	Gas density
ρ_2	Liquid density

$\bar{\rho}$	Mixture density, $\alpha_1\rho_1 + \alpha_2\rho_2$
$\bar{\rho}_k$	Averaged density of k-phase
$\langle\rho^2\rangle$	$\alpha_1\alpha_2\rho_1\rho_2 + A_a\,(\alpha_1\rho_1 + \alpha_2\rho_2)$
σ	Surface tension
$\bar{\bar{\tau}}_k$	$2\,\mu_k^e\,\bar{\bar{D}}$, extra stress tensor
$\bar{\bar{\Omega}}_k$	Injected momentum flux density
ω	Angular velocity

List of Figures

List of Table

1. Introduction

This work is mainly concerned with liquid fuel transfer in space, i.e., in zero gravity. A number of concepts for liquid transfer between "sender" and "receiver" tanks in a zero-gravity environment have been proposed [1]. All of these are concerned in part with the problem of collecting the liquid phase and feeding it to a pumping unit while providing for the return of gases from the receiver tank to the sender tank. The major difference between the fuel transfer in space and that on earth is the absence of body forces in space. Thus, there is no natural orientation of the liquid and vapor in a tank.

The transfer of fuel by pumping requires separation of the liquid and gas. The basic requirement is to orient/collect the liquid to be transferred in the sender tank and to provide the vent system in the receiving tank to prevent excessive liquid loss. Depending on different situations, there are several techniques used to separate liquid from gas in order to optimize the transfer process.

Positive displacement, linear acceleration, tumble acceleration, roll acceleration, centrifugal fluid motion, dielectrophoresis, acoustic, and magnetic forces, and surface tension, etc. are the most common techniques referred [1]. Each technique has its own shortcoming. For example, rotation of the entire vehicle and receiver was not considered practical due to adverse dynamic effects and changing center of gravity while transferring. Rotation of the tankage within the vehicle was not desirable due to the requirement for stationary to rotational connections. An alternative to the roll acceleration method is to create a centrifugal motion in the fluid while holding the vehicle system stable.

Fluid rotation can be provided by various mechanical systems or by fluid injection. The main disadvantages of mechanical systems are their requirements for motor drives and potentially higher residual weights (e.g., long diameter paddles that would sweep liquid away from the wall while short diameter paddles might not be effective for partially filled tanks). Therefore, in this report, fluid rotation created by fluid injection is considered.

The centrifugal forces created by vortex motion have been used for various separation applications. The hydrocyclone used to separate solid particles via specific gravity differences is a very economical hydraulic device with no moving parts. However, some basic questions are:

(1) Can a vortex motion be used practically to orientate the fuel location for fuel transfer in zero gravity?

(2) If so, can it do the job more effectively than other methods?

To answer these questions, one requires a more complete understanding of the hydraulic characteristics of two-phase vortex motion. Normally the residuals are dependent on the volumetric, pump-out flowrate from the tanker. Intuition suggests that one should set a desirable acceleration level for pump-out, select the optimum flow rate and control this flow rate toward the end of the transfer time. The basic approach is to determine at what rate the fluid must be rotated to insure liquid at the wall. Thus, it is desirable to properly describe the pertinent flow processes and to produce the proper set of equations that can be manipulated and solved to give the necessary answers for design purposes.

To help in answering the above questions and to provide design guidance, we have developed a physical/mathematical model for the fluid dynamical behavior of liquid-gas flow in a cylindrical tank at zero-gravity.

The general objectives of the study are: 1) to develop a computer model for a two-phase vortex motion at zero-gravity; 2) to study fluid dynamical behavior of the two phase in the sender tank; 3) to provide a mathematical framework containing the essential physical mechanisms on vortex induced phase-separation; 4) to provide quick/easy sensitivity tests on various parameters; and 5) to provide guidance for the design and testing of MIST (Mechanically Induced Settling Technology) transfer systems, and their scale-up to appropriate sizes.

2. Transfer Concept and Mode of Operation

The MIST Transfer Concept recently proposed by KSC-NASA uses fluid induced rotation (vortex motion) to establish an annular region of the liquid phase adjacent to the walls of a cylindrical tank.

Figure 1 presents a simplified diagram of the MIST Transfer System. Initially, the gas and liquid phases in the sender tank are arbitrarily distributed. During the start-up stage, the liquid will be centrifuged outwardly while the gas will move radially inward. The time required to reach continuous liquid transfer will vary depending upon the initial distribution of phases. To provide for optimum operation of the MIST transfer system and reliable design and scale-up, the fluid dynamical behavior of the fluids in the sender tank must be properly modeled. In this work, the objective was to estimate a characteristic measure of this time, but no attempt was made to model the detailed fluid dynamics during start-up.

Optimum performance, in the sense of minimized pumping time, may require interactive control of the overall pumping rate. Ideally, the flow in the sender tank is divided into two regions. A central gas core-defined

by a single gas-liquid interface is surrounded by a liquid annulus containing a dispersed gas phase. Sufficient vortex rotation in the sender tank must be maintained to provide the radial pressure gradient necessary to transport the gas bubbles from the wall region toward the interface and the liquid from the tank core region toward the wall. If the rotation is too weak gas bubbles will be drawn into the MIST unit along with the liquid. On the other hand, intense rotation produced by a high pumping rate could produce a sufficiently high speed injection rate that the injected fluid will travel along the wall directly to the MIST unit collection point. The optimum pumping rate can be determined by modeling the flow in the sender tank during the continuous stage of operation.

2.1 Early Transfer Concept

During the early stages of this study, a slightly different operational mode was proposed. In this mode, the vortex motion was established and maintained by tangential gas injection at the wall as illustrated schematically in Figure 1. Interfacial momentum transfer from the gas phase to the liquid phase was the principal mechanism sustaining the overall annular vortex flow pattern illustrated in Figure 2.

The transfer process was controlled by the MIST unit illustrated in Figure 1. Two stages of operation could be identified. During start-up, the MIST unit drew an initially arbitrary mixture of liquid and gas from the sender tank, separated the phases, sent the liquid phase to the receiver tank, and returned the gas phase to the sender tank through the tangential injection system (MIST unit). The returning gases initiated rotation of the tank contents. Once the annular liquid region shown in Figure 2 is established, a valve closed in the gas return line of the MIST unit and

liquid was continuously transferred by the MIST unit to the receiver tank. During this continuous stage of operation gas, displaced by the liquid in the receiver tank, was transferred to the sender tank through the tangential injection system and sustained the vortex motion.

After preliminary study established a general understanding of the overall flow mechanics, i.e., the integral momentum balances involved, the conclusion was drawn that this early transfer concept should be somewhat modified. The modification made was mainly in procedure rather than in hardware.

Conceptually, the problem with driving the liquid vortex with an incoming stream of vapor and extracting a stream of (mostly) liquid is that more angular momentum is being withdrawn from the tank than is being introduced. This is due to the large density difference between the two streams. The overall decrease of angular momentum will cause the vortex to slow down, increasing the likelihood that gas bubbles will be drawn into the outlet stream. Though the flow in the tank is complicated, it would seem likely that the rotating flow could not even be initiated using this approach.

Although the incoming angular momentum can be increased by modifying the inlet nozzle geometry, an extreme difference in the nozzle geometries would be required to maintain a constant angular momentum due to the large density difference between gas and liquid phases. Additionally, viscous losses will further increase the loss of angular momentum. Loss of angular momentum in the tank will generally result in a decrease in angular velocity. Thus, the radial pressure gradient, and therefore the centrifugal force on the liquid will be reduced.

2.2 An Alternative Mode of Operation

As the result of the general conclusion drawn above, a somewhat modified mode of operation was proposed. Instead of the single continuous process of injecting gas into the tank while liquid is being pumped out, a two-stage operation may be employed. The first stage - the start-up stage (Figure 3), would return all fluid - liquid and gas that is, pumped from the outlet - back to the inlet. The greater density of the injected fluid would alleviate the momentum loss discussed above and permit the vortex to develop. Eventually, vapor bubbles would migrate to the core of the tank and only liquid would be passed through the pump. When the vortex has sufficient strength (or when a balance of pumping gains and flow losses exists) and a certain phase separation has been achieved, the liquid can be pumped to the receiver tank (Figure 4) and vapor returned to the sender tank (but to the core, not to the perimeter). In this second stage - the pump-out stage, as the liquid is withdrawn, the vortex will lose strength, but since the vapor returns to the core, there is a much reduced risk of entraining bubbles in the outlet until the vortex strength is nearly spent.

A conceptual sketch of how the two-stage "start-up" and "pump-out" model might operate is shown in Figure 5. Schematically, the time evolutions of the vortex strength and the degree of phase separation of the two-stage operation concept are plotted on an arbitrary ordinate scale for the purpose of describing the concept. The definitions and the magnitudes are entirely arbitrary. Nevertheless, the vortex strength can be thought of as the total angular moemntum of the fluids in the tank, whereas the degree of phase separation can be thought of as the liquid volume fraction near the port from which liquid will be withdrawn. Other definitions can also be found in the section on numerical results. Initially, (i.e., at t = 0) the

system is shown to have zero vortex strength and an arbitrary level of phase separation. During the start-up stage, ($0 < t < t^*$) due to fluid injection action, the vortex is growing and its strength is increasing with time. The radial pressure gradient produced by the vortex motion will promote the light gas to move inwardly and the heavy liquid to move outwardly and the degree of phase separation is thus increasing with time. As the vortex motion reaches a sufficient strength, additional injection action may no longer be very effective because higher velocities would be required. At this time, the injecting action can be either reduced or stopped. In the mean time, the separation process continues because of the existing vortex motion. Once the degree of separation has progressed beyond the critical value, (e.g., at time = t^*), the pump-out stage, in which the liquid transfer from the sender tank to the receiver is done, can be started. Critical separation levels (as one being shown in Fig. 5) can be determined according to various criteria. As the pump-out (transfer) stage proceeds ($t^* < t < t^{**}$), the vortex strength will decrease by virtue of the liquid being pumped out from the annular layer at the cylinder wall and the degree of separation can either increase or decrease depending on the strength of the remaining vortex and the pumping conditions. When the degree of separation reduces to the critical phase separation (e.g., time = t^{**}), the transfer is no longer practical due to the small volume fraction of liquid being able to be transferred, and the transfer process stops. The liquid residual in the sender tank when the transfer is stopped is another design parameter and should be made as small as possible. It can sometimes be reduced by increasing the vortex strength and/or by decreasing the pump-out rate.

As discussed above, a two stage operational mode is proposed in this study. Figure 6 shows the configuration of the modified two-stage MIST Transfer System. During the start-up stage, $Q_2 = Q_4 = 0$, and $Q_1 = Q_3$. That is, all fluids withdrawn are returned to the sender tank. The flow dynamics in the sender tank during this stage are those of the pertinent two-phase flow situation. This stage is employed to develop an active vortex such that the separation of liquid from vapor bubbles can be initiated and ultimately achieved. In the transfer stage, $Q_1 \approx Q_2$, $Q_3 \approx Q_4 \approx 0$ and the flow could be treated as a single phase-liquid, pump-out problem. To insure an optimal liquid transfer, a sufficiently high degree of phase separation during the pump-out stage needs to be maintained. For some cases, if the vortex loses too much strength either due to a large pump-out rate or due to friction during the pump-out stage, a small amount of the pumped liquid, Q_3 could be recirculated back to the sender tank to maintain sufficient vortex angular momentum. Also, any gas, Q_4 picked up and separated by the MIST unit will be sent back to the core.

2.3 Start-Up (Spin-Up) Stage

During the start-up period, since all fluid pumped out is returned to the tank, the mass of fluid inside the tank remains unchanged. However, due to the action of the external pump and its injection action, the total angular momentum (or vortex strength) is increasing with time. Since a jet at a larger radial location produces a larger angular momentum for the same linear jet speed, the inlet nozzle should be located near the perimeter. Also, since a mixture with a higher liquid volume fraction has higher mass density thus producing higher angular momentum, the outlet nozzle should

also be located near the perimeter where a higher liquid volume fraction is expected.

Referring to Figure 6, the net change of angular momentum (or vortex strength) of the system due to injection action can be estimated by

$$\frac{dM_a}{dt} = R(m_3 V_j - m_1 V),$$

where R is the radius of the tank, m_i is the mass flow rate at the port location i, V is the vortex speed, and V_j is the injected jet speed. Thus, as expected, in order to increase the vortex strength, the jet speed should be larger than the vortex speed, i.e., $V_j > V$ since $m_1 = m_3$. In fact, unless the jet speed is larger than the local vortex speed, the angular momentum of the system will normally decrease with time and the desired rotational motion could not even be initiated. This is due to two facts. First, during this period, it is expected that the lighter vapor bubbles would migrate to the core of the tank and the average density near the wall will increase with time. Thus, a slight time lag for the mixture to get to the inlet nozzle from the outlet nozzle normally implies $m_3 < m_1$. Again, this means more angular momentum is being withdrawn from the tank than is being introduced if $V_j = V$. Secondly, fluid viscosity will further reduce the total angular momentum of the system.

Some characteristic features to be noted during the start-up stage can be summarized below:

i) The fluid is a two-phase one - where each plays a significant role;

ii) All of the fluid mixture which is pumped out is returned to the tank ($Q_1 = Q_3$, $Q_2 = Q_4 = 0$);

iii) Both inlet and outlet nozzles are located near the tank perimeter;

iv) The injected jet speed should be larger than the local vortex speed to increase the net angular momentum.

2.4 Pump-Out (Transfer) Stage

After the vortex has sufficient strength and the spin-up time is sufficiently long, the separation of liquid and vapor can be established according to specified criteria. At this condition (i.e., $t = t^*$, see Fig. 5), the liquid forms an annulus against the wall of the tank and around a core of vapor, and the second operational stage, the transfer stage, can begin. In this, single phase liquid, Q_1 can be pumped out from the tank perimeter, and vapor from the receiver tank returned to the center core of the sender tank, see Fig. 6. During this process the total angular momentum will decrease. To maintain a reasonable vortex strength, a small amount of high speed liquid, Q_3, could be pumped in at the perimeter. Thus, the transfer stage is mainly a single-phase flow with a central vapor core.

Some characteristics of the transfer stage are:

i) There is an interfacial radius R_c between the vapor core and the liquid annulus; gas is present only for $r < R_c$; liquid is present only for $r > R_c$;

ii) Inlet vapor flows into the center core and outlet liquid flow, Q_1 occurs at the tank perimeter;

iii) If needed, a small inlet liquid flow, Q_3 can occur at the tank perimeter with an inlet jet speed $V_j > V$;

iv) $Q_4 \approx 0$, and transfer rate $Q_2 = \frac{d}{dt}(\pi R_c^2)$

$$\text{or } R_c^2 = \int \frac{Q_2}{\pi} dt + R_{co}^2$$

where R_{co} is the initial interfacial radius of the transfer stage.

v) Total angular momentum in tank M_a is

$$M_a = 2\pi[\rho_1 \int_o^{R_c} r^2 V \, dr + \rho_2 \int_{R_c}^{R} r^2 V \, dr]$$

and also

$$\frac{dM_a}{dt} = \rho_2 R (Q_3 V_j - Q_1 V)$$

If, $Q_3 = 0$, and $V = r\omega$, we have

$$M_a = \frac{\pi\omega}{2}[(\rho_1 - \rho_2) R_c^4 + \rho_2 R^4]$$

and

$$\frac{dM_a}{dt} = -\rho_2 R^2 \omega Q_1$$

Thus, we have

$$\frac{\dot{\omega}}{\omega} = \frac{-2 Q_1 [(\rho_1 - \rho_2) R_c^2 + \rho_2 R^2]}{[(\rho_1 - \rho_2) R_c^4 + \rho_2 R^4] \pi}$$

$$\ell n(\frac{\omega}{\omega_o}) = -\frac{2}{\pi} \int_o^t \frac{Q_1[(\rho_1 - \rho_2) R_c^2 + \rho_2 R^2]}{(\rho_1 - \rho_2) R_c^4 + \rho_2 R^4} dt$$

Since $\rho_1 << \rho_2$, the vortex velocity becomes

$$\ell n(\frac{\omega}{\omega_o}) = \frac{2}{\pi} \int_o^t \frac{Q_1 dt}{(R^2 + R_c^2)} = -2 \int_{R_{co}}^{R_c} \frac{dR_c^2}{R^2 + R_c^2}$$

$$\frac{\omega_o}{\omega} = (\frac{R^2 + R_{co}^2}{R^2 + R_c^2})^2 = [1 + \frac{\int_o^t Q_1 dt}{\pi (R^2 + R_{co}^2)}]^2$$

This equation describes the decrease of the angular velocity of the vortex as the transfer is taking place.

The pressure at the tank wall P_w is another important quantity. It can be estimated in the vortex flow where the radial velocity is much smaller than tangential velocity. Integration of pressure gradient equation $\frac{\partial p}{\partial r} = \rho v \omega^2$ gives

$$P_w = P_c + \frac{\omega^2}{2} [\rho_1 R_c^2 + \rho_2 (R^2 - R_c^2)]$$

$$= P_c + \frac{\rho_2 \omega^2}{2} (R^2 - R_c^2) \quad \text{if } \rho_1 << \rho_2$$

$$= P_c + \frac{\omega_o^2 \rho_2}{2} (R^2 - R_{co}^2 - \int \frac{Q_1 dt}{\pi}) [1 + \frac{\int_o^t Q_1 dt}{\pi (R^2 + R_{co}^2)}]^{-4}$$

where P_c is the pressure at center core. If P_c is kept constant, the wall pressure P_w will decrease as the transfer stage continues. It is also noted that the viscous stress on the cylinder wall will further decrease the vortex strength ω, and thus reduce further the wall pressure. Reduced wall pressure implies the pump will have to pump harder to withdraw the liquid.

3. Modeling of Start-up Stage

The physical/mathematical model for the start-up stage will be based on the two-phase, two fluid continuum hypothesis. The work considers the flow in the sender tank to be specified by the tank geometry, fluid properties, nozzle geometry and the overall pumping rate (the volume flow rate of the mixture in the tangential injection system). The flow in the sender tank is assumed to be two-dimensional with no flow and no gradients along the length (axis of symmetry) of the tank. The fluid injection system is modeled as a direct line source for tangential injection and fluid withdrawal is modeled as a line sink. Although the cryogenic fluids of most interest in space operations exhibit significant interfacial mass transfer, the fluid motion is driven principally by the interfacial momentum transfer from the injected fluid mixture to the fluids in the tank. Therefore, our analysis assumes zero interfacial mass transfer as would be closely approximated by an air-water system. Both phases are assumed incompressible. Surface tension between the fluids is assumed to be negligibly small compared to the other interfacial forces.

3.1 General Formulation

The two-fluid or separated flow model is one of several classes of possible approaches to the analysis of two-phase flow [2]. It is based on separate conservation equations of mass, momentum and sometimes energy in two-phase flow for each phase. This model seems to be especially suitable for the uniformly dispersed two-phase flow. Various forms of the system of equations for two-fluid two-phase flow may be found elsewhere [3-9]. Many of these are obtained via postulating macroscopic qualities without reference to microscopic relations; others are formulated more rigorously

and systematically by averaging the microscopic equations. Some of these are good only for special cases and are more practical; others are more general but are usually too complicated to be practical. Nevertheless, all of them seem to have retained the expressions for the phase interactions, i.e., additional source terms or closure laws.

The basic time-dependent fluid dynamical equations consist of averaged equations of motion for each phase, and two continuity equations written in terms of the volume fraction. Here we will give briefly the formulation of the system equations. For a detailed review of this formulation, the reader is referred to the paper of Drew [6].

In the interior of each phase, the equations of motion are

$$\frac{\partial \rho_k}{\partial t} + \nabla \cdot \rho_k \bar{V}_k = 0 \tag{1}$$

and

$$\frac{\partial \rho_k \bar{V}_k}{\partial t} + \nabla \cdot \rho_k \bar{V}_k \bar{V}_k = \nabla \cdot \bar{\bar{T}}_k + \rho_k \bar{B}_k \tag{2}$$

At the interface, jump conditions are written via conservation of mass and momentum as

$$\sum_k \rho_k (\bar{V}_k - \bar{V}_i) \cdot \bar{n} = 0 \tag{3}$$

and

$$\sum_k [\rho_k \bar{V}_k (\bar{V}_k - \bar{V}_i) - \bar{\bar{T}}_k] \cdot \bar{n} = \sigma \kappa \bar{n} \tag{4}$$

Here ρ is density

$\bar{V}$ is the velocity

$\bar{\bar{T}} = - p \bar{\bar{I}} + \bar{\bar{\tau}}$ is the total stress tensor

p is the pressure

$\bar{\bar{\tau}}$ is the extra stress tensor

$\bar{\bar{I}}$ is the unit tensor

$\bar{B}$ is the body force density

$\bar{V}_i$ is the interfacial velocity

σ is the surface tension

κ is the curvature of the interface

$\bar{n}$ is the unit vector normal to the interface and the subscript $k = 1$ and 2, denotes gas and liquid phases, respectively.

Although the equations in the interior of each phase are well known, the interface conditions between two phases are quite complicated. That is, the essential difficulty in the two-fluid formulation comes from the presence of moving interfaces and the interfacial mass and momentum transfers. When one considers the local (microscopic) flow properties, the shape and velocity of the interfaces is not known a priori. Due to the complication of the detailed interfacial properties, solving the local instant variables of the flow field based on the system of equations in the interior of each phase would result in an intractable (and thus - hopeless) multi-boundary problem except in the most academic examples. Thus, as in the field of turbulence, the method of the averaged process is adopted to study this complicated two-phase flow.

Referring to Ref. 6, the averaged equations can be written as

$$\alpha_1 + \alpha_2 = 1 \tag{5}$$

$$\frac{\partial \alpha_k}{\partial t} + \nabla \cdot \alpha_k \bar{V}_k = 0 \tag{6}$$

and

$$\alpha_k \rho_k \frac{d\bar{V}_k}{dt} = - \alpha_k \nabla p_k + \nabla \cdot \alpha_k \bar{\bar{\tau}}_k + \alpha_k \rho_k \bar{B}_k + \bar{M}_k \tag{7}$$

with

$$\bar{M}_1 + \bar{M}_2 = 0 \tag{8}$$

and

$$\frac{d\bar{V}_k}{dt} = \frac{\partial \bar{V}_k}{\partial t} + \bar{V}_k \cdot \nabla \bar{V}_k$$

is the total derivative of the velocity $\bar{V}_k$.

Here, all the quantities are referred to as the averaged macroscopic values, α_k is the volume fraction, $\bar{\bar{\tau}}_k$ is the total effective extra stress tensor, and $\bar{M}_k$ is the effective interfacial force density of the k-phase.Eq. (8) merely states that the interfacial forces with opposite signs in the momentum equations balance between the separate phases. That is, the interfacial force is just an internal force for the mixture and will not appear in the equation of motion for a mixture. Thus, from equation (7), the mixture momentum equation is

$$\sum_k \alpha_k \rho_k \frac{d\bar{V}_k}{dt} = -\nabla p + \nabla \cdot \left(\sum_k \alpha_k \bar{\bar{\tau}}_k\right) + \sum \alpha_k \rho_k \bar{B}_k \tag{9}$$

where the interfacial force has been eliminated.

In order to obtain the averaged system of equations several assumptions have been made. Among those are:

i) Constant physical properties for each phase, i.e., ρ_k, μ_k are constant.

ii) Each phase is treated as an incompressible fluid and there is no pressure jump inside each phase.

iii) No phase change between phases, i.e., there is no interfacial mass transfer.

iv) Neither heat transfer nor thermodynamics is considered.

v) The physical/mathematical model is based on the two-phase continuum hypothesis. The initial approach is to assume a bubbly flow regime.

Furthermore, the surface tension (or the contact pressure) is neglected, and there is no pressure difference between the phases. Thus, only one pressure variable is all we need, and equations (6) and (7), with

$$p_1 = p_2 = p,$$

describe the system dynamics provided the variables $\bar{\bar{\tau}}_k$ and $\bar{M}_k$ can be expressed in terms of the local state variables.

Our averaging process eliminates complex formulations for the microscale fluctuations around the bubbles or droplets. This process has lumped the effects of the interfacial interactions between phases into the effective stress tensor $\bar{\bar{\tau}}_k$ and the effective interfacial force, $\bar{M}_k$. In order to properly model a two-phase flow, the constitutive equations for the averaged stress tensor $\bar{\bar{\tau}}_k$ and the interfacial force density $\bar{M}_k$ need to be given.

In general, both $\bar{\bar{\tau}}_k$ and $\bar{M}_k$ could be functions of various parameters, such as ρ_k, μ_k, $\bar{V}_k$, d_k, $\frac{d\bar{V}_k}{dt}$, .. etc., in a very complicated way. In modeling the averaged stress tensor $\bar{\bar{\tau}}_k$, an analogy in certain aspects

between single-phase and two-phase flow is assumed. As given in Refs. (6, 10), the stress tensor due to fluctuations, $\bar{\bar{\tau}}_k$ is modeled by the effective viscosity and the mean deformation tensor as

$$\bar{\bar{\tau}}_k = 2\,(\mu_k + \mu_k^t)\,\bar{\bar{D}}_k = \mu_k^e\,(\nabla\bar{V}_k + \bar{V}_k\nabla) \qquad (10)$$

where μ_k, μ_k^t and $\mu_k^e = \mu_k + \mu_k^t$ are the dynamic viscosity, the turbulent eddy viscosity, and the total effective viscosity, respectively. Although there are several models for the eddy viscosity for single phase flow, few correlations for the eddy viscosity in two-phase flow can be found in the literature. In reference 10, the fluctuations of the turbulent velocity, and thus the turbulent eddy viscosity μ_k^t, in two-phase flow had been assumed to be due to two distinct mechanisms: (1) momentum exchange of the liquid phase, and (2) movement of the dispersed phase. A proper modeling of the total effective viscosity μ_k^e in a complex two-phase flow requires further study. In this report a constant effective viscosity is assumed.

The modeling of the interfacial force density $\bar{M}_k$ is much more involved because the interfacial forces which result from the averaging process are, in general, very complicated. Many investigators [4, 9, 11-15] have devoted considerable effort to define or model these interactions. The most common effects included are the classical drag forces, the forces due to the relative acceleration or the so called added mass forces, the lift forces, the Basset memory forces, etc. Here we assume that the interface forces are dominated by the classical drag and added mass terms as:

$$\bar{M}_1 = A_d(\bar{V}_2 - \bar{V}_1) + A_a \frac{d}{dt}(\bar{V}_2 - \bar{V}_1) \qquad (11)$$

the first term represents the classical drag forces and the second term is the force due to the relative acceleration.

With the aid of the constitutive equations (or closure laws) for the total stress (eq. 10) and for the interfacial forces (eq. 11), equations (5), (6) and (7) now describe the system dynamics of our two-phase, two fluid problem. The nine equations provide a set of equations in the nine variables $\bar{V}_k$ (6 variables), α_k (two variables), and p. They are thus the equations required to provide a mathematical description of the two phase flow system in terms of local mean variables.

From equations (5) and (6), an important incompressible condition is obtained

$$\sum_k \nabla \cdot \alpha_k \bar{V}_k = \nabla \cdot \sum_k (\alpha_k \bar{V}_k) = o \qquad (12)$$

Equation (12) is analogous to the important condition of $\nabla \cdot \bar{V} = o$ for incompressible single phase flow. It should be emphasized here that in a two-phase flow, the condition of $\nabla \cdot \bar{V}_k = o$ is no longer true even though the fluid is assumed to be incompressible for each phase (i.e., ρ_k = constant).

The equations of the two-phase model are coupled by the interface forces. Although both the drag and added mass forces are providing the coupling effect between the phases, the inclusion of the added mass in the interfacial forces make the momentum equation behavior much more complicated. This is because the effects due to these two forces are somewhat different. In regard to the system of differential equations, the drag force is just an algebra term and does not alter the characteristic of

the differential equations; whereas the added mass force involving the total derivatives does modify the characteristics of the differential equations.

By substituting the interfacial forces, eq. (11), into equation (7), we have

$$\rho_1\alpha_1 \frac{d\bar{V}_1}{dt} = -\alpha_1\nabla p + \nabla \cdot \alpha_1\bar{\bar{\tau}}_1 + \alpha_1\rho_1\bar{B}_1 - A_d\,(\bar{V}_1 - \bar{V}_2) - A_a(\frac{d\bar{V}_1}{dt} - \frac{d\bar{V}_2}{dt}) \qquad (13)$$

and

$$\rho_2\alpha_2 \frac{d\bar{V}_2}{dt} = -\alpha_2\nabla p + \nabla \cdot \alpha_2\bar{\bar{\tau}}_2 + \alpha_2\rho_2\bar{B}_2 - A_d\,(\bar{V}_1 - \bar{V}_2) - A_a(\frac{d\bar{V}_1}{dt} - \frac{d\bar{V}_2}{dt}) \qquad (14)$$

where

$\frac{d(\ )}{dt} = \frac{\partial(\ )}{\partial t} + \bar{V} \cdot \nabla (\ \ )$ is the total derivative operation.

Since the addition of the added mass terms has modified the characteristics of the equations, the method of solving the system can be modified correspondingly. Before solving the new system of the differential equations, it is logical to search and rearrange the dynamic equations (13) and (14) into a more convenient form. An additional motivation to search a new, more generalized form stems from the important continuity condition of the two-phase flow, eq. (12).

We can rewrite eqs. (12) and (13) as:

$$(\rho_1\alpha_1 + A_a) \frac{d\bar{V}_1}{dt} + A_a \frac{d\bar{V}_2}{dt} = -\alpha_1\nabla p + \nabla \cdot \alpha_1\bar{\bar{\tau}}_1 + \alpha_1\rho_1\bar{B}_1 - A_d\,(\bar{V}_1 - \bar{V}_2) \qquad (15)$$

$$(\rho_2\alpha_2 + A_a) \frac{d\bar{V}_2}{dt} + A_a \frac{d\bar{V}_2}{dt} = -\alpha_2\nabla p + \nabla \cdot \alpha_2\bar{\bar{\tau}}_2 + \alpha_2\rho_2\bar{B}_2 - A_d\,(\bar{V}_1 - \bar{V}_2) \qquad (16)$$

Thus from Eq. (15) x $(\rho_2\alpha_2 + A_a)$ + Eq. (16) x A_a, we have

$$[\rho_1\rho_2\alpha_1\alpha_2 + A_a\,(\rho_1\alpha_1 + \rho_2\alpha_2)]\,\frac{d\bar{V}_1}{dt} = -\,(\alpha_1\alpha_2\rho_2 + A_a)\nabla p$$

$$+\,(\rho_2\alpha_2 + A_a)\,(\nabla \cdot \alpha_1\bar{\bar{\tau}}_1 + \alpha_1\rho_1\bar{B}_1)$$

$$+\,A_a\,(\nabla \cdot \alpha_2\bar{\bar{\tau}}_2 + \alpha_2\rho_2\bar{B}_2) \qquad (17)$$

$$-\,\rho_2\alpha_2 A_d\,(\bar{V}_1 - \bar{V}_2)$$

and from Eq. (15) x A_a + Eq. (16) x $(\rho_1\alpha_1 + A_a)$ we have

$$[\rho_1\rho_2\alpha_1\alpha_2 + A_a\,(\rho_1\alpha_1 + \rho_2\alpha_2)]\,\frac{d\bar{V}_2}{dt} = -\,(\alpha_1\alpha_2\rho_1 + A_a)\nabla p$$

$$+\,(\rho_1\alpha_1 + A_a)\,(\nabla \cdot \alpha_2\bar{\bar{\tau}}_2 + \alpha_2\rho_2\bar{B}_2)$$

$$+\,A_a\,(\nabla \cdot \alpha_1\bar{\bar{\tau}}_1 + \alpha_1\rho_1\bar{B}_1) \qquad (18)$$

$$+\,\rho_1\alpha_1 A_d\,(\bar{V}_1 - \bar{V}_2)$$

Equations (17) and (18) can be written into a generalized equation as:

$$\frac{d\bar{V}_k}{dt} = -\,C_{pk}\,\nabla p + \sum_{\ell=1}^{2} C_{k\ell}\,(\nabla \cdot \alpha_\ell\bar{\bar{\tau}}_\ell + \rho_\ell\alpha_\ell\bar{B}_\ell) + C_{dk}\,(\bar{V}_1 - \bar{V}_2) \qquad (19)$$

where the generalized coefficients are

$$C_{p1} = (\alpha_1\alpha_2\rho_2 + A_a)/\langle\rho^2\rangle$$

$$C_{p2} = (\alpha_1\alpha_2\rho_1 + A_a)/\langle\rho^2\rangle$$

$$C_{11} = (\alpha_2\rho_2 + A_a)/\langle\rho^2\rangle$$

$$C_{12} = C_{21} = A_a/\langle\rho^2\rangle \qquad (20)$$

$$C_{22} = (\alpha_1\rho_1 + A_a)/\langle\rho^2\rangle$$

$$C_{d1} = -\alpha_2\rho_2 A_d/\langle\rho^2\rangle$$

$$C_{d2} = \alpha_1\rho_1 A_d/\langle\rho^2\rangle$$

and

$$\langle\rho^2\rangle = \alpha_1\alpha_2\rho_1\rho_2 + A_a\,(\alpha_1\rho_1 + \alpha_2\rho_2)$$

Also

$$\alpha_\kappa \frac{d\bar{V}_k}{dt} = \frac{\partial\, \alpha_k\bar{V}_k}{\partial t} + \nabla \cdot \alpha_k\bar{V}_k\bar{V}_k \qquad (21)$$

Thus, equations (5), (6) and (19) are the generalized system of equations.

The major advantages of writing the momentum equations in the generalized form of eq. (19) are the following. First, the generalized equation is similar to the well known Navier-Stokes equation. Second, by using eq. (19) and the continuity condition for two-phase flow, eq. (12), a

Poisson type equation for pressure field can be obtained. Thus, the existing techniques can be used to solve this system of equations, and the pressure field can be determined through the local independent variables. To do this, taking the divergence of the sum of equations (19), we have

$$\nabla \cdot (\alpha_1 C_{p1} + \alpha_2 C_{p2}) \nabla p = - \nabla \nabla \cdot \Sigma \alpha_k \overline{V}_k \overline{V}_k$$

$$+ \nabla \cdot \sum_k \left[\sum_\ell \alpha_k C_{k\ell} \left(\nabla \cdot \alpha_\ell \overline{\overline{\tau}}_\ell + \alpha_\ell \rho_\ell \overline{B}_\ell \right) \right.$$

$$\left. + \alpha_k C_{dk} (\overline{V}_1 - \overline{V}_2) \right] \qquad (22)$$

since

$$\nabla \cdot \Sigma \frac{\partial \alpha_k \overline{V}_k}{\partial t} = o \text{ from eq. (12).}$$

3.2 Interfacial Force Coefficients

The modeling of the interfacial forces is one of the most challenging tasks facing those involved with the two-phase flow problems. As discussed before, the classical drag and added mass terms are the most common and important contributions cited in the literature. Our discussion which follows will be limited only to these two forces. In fact, even for these classical forces, there are various expressions used in the literature [4, 6, 9, 12, 14]. However, all of these expressions are developed and tested only for dilute, two-phase cases.

Before modeling the interfacial forces, it is important to discuss the average bubble or droplet size. The reason for this is that the two-phase, two fluid model basically assumes the flow field to be in the uniformly

bubbly or in the uniformly dispersed droplet flow regime and that the interfacial forces are greatly dependent on the size of bubbles or droplets. The importance of the bubble sizes on the drag forces can easily be seen in the following discussion. To be more realistic, the average size, d_k should be allowed to vary in the flow field and in general should be functions of various parameters including the local turbulence intensity, mixing, and the volume fraction, α_k, since all these quantities will affect the break-up and coalesce of the bubbles or droplets. To discuss the volume fraction effect, where n_k is the particle (bubble) number density of phase k, we have $\alpha_k = n_k \pi d_k^3/6$. And if $d_k \sim \alpha_k$ (i.e. $d_k = d_{ok}\alpha_k^{\gamma}$) then $n_k \sim \alpha_k^{1-3\gamma}$. Since one might expect that both n_k and d_k will increase as α_k increases, we have $0 < \gamma < 1/3$. The size variations as functions of gas volume fraction, α_1 for $\gamma = 0.2$ and $d_{01} = d_{02} = 1$ cm are shown in Fig. 7. Although these are the typical values used in the test runs, it is noted that other expressions can easily be put into the program. After having the size information, the interfacial forces can be modeled. For dilute bubbles dispersed in a continuous liquid, the drag and added mass coefficients, A_{d1} and A_{a1} are generally expressed as [6, 12, 14]

$$A_{d1} = \frac{3\alpha_1\rho_2}{4d_1} C_D \left|\bar{V}_1 - \bar{V}_2\right|$$

and

$$A_{a1} = \alpha_1\rho_2 \left(\frac{1}{2} + \frac{3}{2}\alpha_1\right)$$

Here the bubble particles are assumed to remain spherical,

$$C_D = 24\ (1 + 0.1\ Re^{3/4} + \ldots)/Re$$

via the Oseen drag coefficient [11], where

$$Re = \frac{\rho_2 d_1 |\bar{V}_1 - \bar{V}_2|}{\mu_{2m}} \text{ , and } \mu_{2m} = \mu_2/\alpha_2.$$

Here, d_1 is the averaged diameter of the dispersed bubbles. If the Stoke's drag is used (i.e. $C_D = 24/Re$) then the drag coefficient becomes

$$A_{d1} = \frac{18\mu_2\alpha_1}{d_1^2\,\alpha_2} \tag{23}$$

which is independent of the velocity field. Also, since the upper bound of the added mass coefficient should not exceed $\alpha_2\rho_2$ which corresponds to carrying all of the continuous liquid with the bubble during its acceleration, a modified added mass coefficient is assumed to be

$$\frac{1}{A_{a1}} = \frac{1}{\alpha_1\rho_2(\frac{1}{2} + \frac{3}{2}\,\alpha_1)} + \frac{1}{\alpha_2\rho_2} \tag{24}$$

On the other hand, if one considers that the two-phase flow consists of liquid drops dispersed in a continuous gas flow field, a second set of the coefficients can be expressed:

$$A_{d2} = \frac{18\,\alpha_2\,\mu_1}{(1-\alpha_2/0.8)^2 d_2^2} \tag{25}$$

and

$$\frac{1}{A_{a2}} = \frac{1}{\alpha_2 \rho_1 (\frac{1}{2} + \frac{3}{2}\alpha_2)} + \frac{1}{\alpha_1 \rho_1} \tag{26}$$

where the maximum percentage of 0.8 for droplets in gas is assumed.

Now we have two sets of expressions for the added mass and drag coefficients, but no existing criteria to determine which set of equations should be used for a general two-phase flow problem. As a matter of fact, neither set of the expressions is expected to be good for the entire range of volume fraction. For a dilute gas dispersed in a liquid (i.e. $\alpha_1 \to 0$), the coefficients should approach those of the first set (i.e. A_{d1} and A_{a1}); while for a dilute liquid dispersed in gas (i.e. $\alpha_1 \to 1$) the coefficients should approach those of the second set (A_{d2} and A_{a2}). In general, the value of α_1 could be any value between 0 and 1. Here we will model the coefficients by a weighting technique, and express the coefficient as

$$A_a = A_{a1} w_{a1} + A_{a2} w_{a2} \tag{27}$$

$$A_d = A_{d1} w_{d1} + A_{d2} w_{d2} \tag{28}$$

where w_{a1}, w_{a2}, w_{d1} and w_{d2} are the weighting functions to be selected. Normally, we set $w_{a1} + w_{a2} = w_{d1} + w_{d2} = 1$ and all the weighting functions are functions of the volume fraction α_1. In the model here, we choose

$$w_{a1} = \frac{\alpha_2^{n_a}}{\alpha_2^{n_a} + \alpha_2^{n_a}}, \quad w_{a2} = 1 - w_{a1} \tag{29}$$

$$w_{d2} = \frac{\alpha_2^{n_d}}{\alpha_2^{n_a} + \alpha_2^{n_a}}, \quad w_{a2} = 1 - w_{a1} \tag{30}$$

with $n_a = n_d = 4$.

Fig. 8 shows the dilute drag coefficients A_{d1} and A_{d2} and the modeling drag coefficients A_d. Fig. 9 shows the corresponding added mass coefficients. The modeling coefficients approach those for dilute conditions as should be the case. It should be noted again that different models for the coefficients can be easily adopted.

3.3 Equations in Polar Coordinates

Due to the nature of the problem, it is more convenient to write the system of equations in polar coordinates. For a two-dimensional flow in polar coordinates, some of the useful relations are:

$$\nabla( ) = \frac{\partial( )}{\partial r}\bar{r} + \frac{\partial( )}{r\partial\theta}\bar{\theta}$$

$$\nabla \cdot (\bar{\ }) = \frac{1}{r}\frac{\partial r( )_r}{\partial r} + \frac{\partial( )_\theta}{r\partial\theta}$$

$$\nabla \cdot (\bar{\bar{\ }}) = \left[\frac{1}{r}\frac{\partial r( )_{rr}}{\partial r} + \frac{\partial( )_{\theta r}}{r\partial\theta} - \frac{( )_{\theta\theta}}{r}\right]\bar{r}$$

$$+ \left[\frac{1}{r}\frac{\partial r( )_{r\theta}}{\partial r} + \frac{\partial( )_{\theta\theta}}{r\partial\theta} - \frac{( )_{\theta r}}{r}\right]\bar{\theta}$$

$$\alpha_k \frac{d\bar{V}_k}{dt} = \frac{\partial \alpha_k \bar{V}_k}{\partial t} + \nabla \cdot \alpha_k \bar{V}_k \bar{V}_k \tag{31}$$

$$\tau_{rrk} = 2\ \mu_k^e \frac{\partial V_{rk}}{\partial r}$$

$$\tau_{r\theta k} = \tau_{\theta rk} = \mu_k^e\ r\ \frac{\partial}{\partial r}\ (V_{\theta k}/r)$$

$$\tau_{\theta\theta\kappa} = 2\ \mu_k^e\ V_{rk}/r \tag{32}$$

Thus, equations (6) and (19) become

$$\alpha_1 + \alpha_2 = 1 \tag{5}$$

$$\frac{\partial \alpha_k r}{\partial t} + \frac{\partial r\alpha_k V_{rk}}{\partial r} + \frac{\partial \alpha_k V_{\theta k}}{\partial \theta} = 0 \tag{33}$$

$$\frac{\partial \alpha_k V_{rk} r}{\partial t} + \frac{\partial r\alpha_k V_{rk}^2}{\partial r} + \frac{\partial \alpha_k V_{rk} V_{\theta k}}{\partial \theta} - \alpha_k V_{\theta k}^2 = -\alpha_k C_{pk}\ r\ \frac{\partial p}{\partial r}$$

$$+ \alpha_k \sum_{\ell=1}^{2} C_{k\ell}\ \left(\frac{\partial r\alpha_\ell \tau_{rr\ell}}{\partial r} + \frac{\partial \alpha_\ell \tau_{r\theta\ell}}{\partial \theta} - \alpha_\ell \tau_{\theta\theta\ell} + \alpha_\ell \rho_\ell\ B_{r\ell} r\right)$$

$$+ \alpha_k\ C_{dk}\ r\ (V_{r1} - V_{r2}) \tag{34}$$

$$\frac{\partial \alpha_k V_{\theta k} r}{\partial t} + \frac{\partial r\alpha_k V_{rk} V_{\theta k}}{\partial r} + \frac{\partial \alpha_k V_{\theta k}^2}{\partial \theta} + \alpha_k V_{\theta k} V_{rk} = -\alpha_k\ C_{pk}\ \frac{\partial p}{\partial \theta}$$

$$+ \alpha_k \sum_{\ell=1}^{2} C_{k\ell}\left(\frac{\partial r\alpha_\ell \tau_{r\theta\ell}}{\partial r} + \frac{\partial \alpha_\ell \tau_{\theta\theta\ell}}{\partial \theta} + \alpha_\ell \tau_{r\theta\ell} + \alpha_\ell \rho_\ell B_{\theta\ell} r\right)$$

$$+ \alpha_k\ C_{dk}\ r\ (V_{\theta 1} - V_{\theta 2}) \tag{35}$$

for k = 1 and 2.

For the axisymmetric case, $\frac{\partial}{\partial\theta} = 0$, and we have

$$\alpha_1 + \alpha_2 = 1 \tag{5}$$

$$\frac{\partial r\alpha_k}{\partial t} + \frac{\partial r\alpha_k V_{rk}}{\partial r} = 0 \tag{36}$$

$$\frac{\partial r\alpha_k V_{rk}}{\partial t} + \frac{\partial r\alpha_k V_{rk}^2}{\partial r} - \alpha_k V_{\theta k}^2 = -\alpha_k C_{pk}\, r \frac{\partial p}{\partial r}$$

$$+ \alpha_k \sum_{\ell=1}^{2} C_{k\ell} \left(\frac{\partial r\alpha_\ell \tau_{rr\ell}}{\partial r} - \alpha_\ell \tau_{\theta\theta\ell} + \alpha_\ell \rho_\ell B_{r\ell} r\right)$$

$$+ \alpha_k C_{dk}\, r\, (V_{r1} - V_{r2}) \tag{37}$$

$$\frac{\partial r\alpha_k V_{\theta k}}{\partial t} + \frac{\partial r\alpha_k V_{rk} V_{\theta k}}{\partial r} + \alpha_k V_{rk} V_{\theta k} = \alpha_k \sum_{\ell=1}^{2} C_{k\ell} \left(\frac{\partial r\alpha_\ell \tau_{r\theta\ell}}{\partial r} + \alpha_\ell \tau_{r\theta\ell} + \alpha_\ell \rho_\ell B_{\theta\ell} r\right)$$

$$+ \alpha_k C_{dk}\, r\, (V_{\theta 1} - V_{\theta 2}) \tag{38}$$

for k = 1 and 2. The incompressible condition of eq. (12) reduces to $\alpha_1 V_{r1} + \alpha_2 V_{r2} = Qr/r$, where Q_r is the net radial volumetric flow. In the start-up stage, $Q_r = 0$.

3.4 Initial and Boundary Conditions

Eqs. (33)-(35) are the governing differential equations for the two-phase fluid motion in cylindrical coordinates under zero gravity conditions. To completely define the system, we need to specify both the initial values and the boundary conditions.

The program was developed to accept arbitrary initial conditions. In addition, a few classical initial velocity fields are also provided. All these classical velocity fields have zero radial velocities, i.e. $V_r = 0$ and their tangential velocities are:

1) Pure rotation

$$V_\theta = r\omega$$

where ω is the circular rotation speed.

2) Hammel-Oseen Vortex (H.O.)

$$V_\theta = \frac{1.398\ V_p}{\bar{r}} \left(1 - e^{-1.25643\ \bar{r}^2}\right)$$

3) G. I. Taylor Vortex (G.I.T.)

$$V_\theta = V_p \bar{r} e^{(1-\bar{r}^2)/2}$$

In H.O. and G.I.T. vorticies, $\bar{r} = r/r_p$, r_p is the vortex core or the location of the maximum velocity, and V_p is the maximum velocity. Also when the classical vortex is used, the velocities for both phases are assumed to be the same.

The specification of the initial condition is rather straightforward, while the boundary conditions are much more involved. In general, the mixture could be pumped in and out of the system in a very complicated way. If determining the detailed flow field is the primary interest, detailed boundary conditions should be included. Here, we have tried to simplify the situation somewhat and model the boundary condition via global effects since only the global dynamical behavior of the two-phase flow in the tank is expected to be useful from the model. For example, at the boundary location (i.e. at the inlet or outlet nozzles) the pumped flow conditions are specified by the average volume fraction of the fluid mixture $\bar{\alpha}_k$, the

average pump volume density q_j, the average jet speed V_j, and the effective pump region, $H_j = \int hdR = h\Delta R$, where ΔR is the nozzle width, and h is the effective jet penetration depth. For axisymmetric cases, $h = 2\pi r$. The global values of V_j and q_j could be estimated from pump flow rate Q_j and the nozzle geometry as: $V_j = Q_j/\Delta R$, and $q_j = Q_j/H_j = V_j/h$. Thus, the volume source rate for the k-phase at the nozzle location is

$$q_k = \bar{\alpha}_k \, q_j, \tag{40}$$

and the momentum flux density for the k-phase at the jet location is

$$\bar{\Omega}_k = = \rho_k \bar{\alpha}_k q_j V_j \bar{n} \tag{41}$$

where $\bar{n}$ is the unit vector of the jet.

In general, these source terms should be added to the system of equations at the nozzle location. That is, a volume source term of rq_k for the continuity equation (33) and a generalized momentum flux density of $r\alpha_k \sum_{\ell} C_{k\ell} \, \Omega_\ell \bar{n}$ for eqs. (34) and (35) should be added at the nozzle location.

Since the cylindrical boundary is fixed, the net inlet flow should be zero,

$$\Sigma \, q_k H_j = \Sigma \, Q_j = 0 \tag{42}$$

The summation is taken over all the inlet and outlet nozzles.

In reality, a source or sink is arranged at the nozzle location. However, during the start-up stage the mixture pumped out is injected immediately back into the tank at the nearby location. The net volume or mass in the system is effectively unchanged except for the net change on the angular momentum. Thus, the pump system (withdrawal and injection) during the start-up stage acts as a body force on the mixture at the nozzle location. The net momentum gain during the start-up stage is thus the

momentum introduced into the system minus the local momentum pumped out. Therefore, we will model this pumping dynamic by body forces without considering the mass transfer. That is, in equations (34) and (35),the body force density $\alpha_k \rho_k \bar{B}_k$ will be replaced by the net momentum gain, $\bar{\Omega}_k - \alpha_k \rho_k q_j \bar{V}$ and

$$\alpha_k \rho_k \bar{B}_k r = \alpha_k \rho_k q_j r(V_j \bar{n} - \bar{V}) = \frac{\alpha_k \rho_k V_j}{2\pi} (V_j \bar{n} - \bar{V}) \qquad (43)$$

will be assumed at the nozzle location. So the total net momentum gain due to the pumping is

$$\sum_j \sum_k \int \alpha_k \rho_k V_j (V_j \bar{n} - \bar{V}) \, dr = \sum_j \sum_k \alpha_k \rho_k Q_j (V_j \bar{n} - \bar{V}) \qquad (44)$$

Besides the pump flow condition, the boundary condition at the tank wall is also required. In general, a non-slip condition at the cylindrical wall should be used, (i.e. $\bar{V}_k = 0$ at $r = R$). If the detailed flow field is not expected to greatly affect the global phenomenon of the fuel transfer of the tank system, the shearing stress at the wall could be simulated by a momentum sink (a negative source) near the wall. For example, these wall stresses could be modeled as

$$\tau_{wk} = \alpha_k \nu_k \frac{\partial V_{\theta k}}{\partial r} = \alpha_k \tau_{wk} \qquad (45)$$

where τ_{wk} is similar to a momentum sink at the wall, since $\tau_{wk} < 0$. The condition of no radial velocity at the boundary (i.e. $V_{rk} = 0$ at $r = R$) will be maintained. To avoid a numerical singularity at the origin, a finite center core region was excluded from the analysis. At this inner boundary, a free surface with no radial velocity will be assumed at all times.

3.5 Numerical Method

Equations (5), (33), (34) and (35) comprise the system of equations for an axisymmetric, two-phase fluid flow. The complete solution of these complicated equations can only be obtained through numerical methods. An improved Lax-Wendroff, two-step scheme, (also referred to as MacCormack's method) [16, 17, 18] is adopted for solving this time-dependent problem. This non-centered differencing scheme, using a full step backward prediction and forward correction version, requires no explicit artificial viscosity if a proper stability condition is satisfied. Using this technique for solving fluid flow problems is very efficient and has been in widespread and successful use for some time. It is good both for the time-accurate computation of steady and unsteady flow problems. The general features of the scheme are: i) its explicitly conservative form, ii) it is a two-step predictor-correction type, iii) it is three point, two level - that is, the solution of f_i^{n+1} at level n+1 depends only on three values of f_i^n at level n, and iv) it is second-order accurate in time and in space.

3.5.1 Equations Utilized

Since there are five independent variables (e.g., V_{r1}, V_{r2}, $V_{\theta 1}$, $V_{\theta 2}$ and α_1) for the system, only five independent equations are needed to define the time dependent problem. The equations selected are one continuity equation and four momentum equations. The final solution is thus to find the correct pressure field so that the other continuity equation is satisfied. Also, the condition of equation (5), $\alpha_1 + \alpha_2 = 1$ is used all the time.

For using the MacCormack's numerical technique, the system of equations is expressed in the conservative form as:

$$W_t = F_r + P_r + gG_r + S \tag{46}$$

Here the subscripts (t and r) denote partial differentiation with respect to t and r, respectively, and W, F, P_r, gG_r and S are column matrices with five elements defined as follows. The components of W are:

$$W = r \begin{bmatrix} \alpha_1 V_{r1} \\ \alpha_2 V_{r2} \\ \alpha_1 V_{\theta 1} \\ \alpha_2 V_{\theta 2} \\ \alpha_1 \end{bmatrix} \tag{47}$$

The components of F:

$$F = -r \begin{bmatrix} \alpha_1 V_{r1}^2 \\ \alpha_2 V_{r2}^2 \\ \alpha_1 V_{r1} V_{\theta 1} \\ \alpha_2 V_{r2} V_{\theta 2} \\ \alpha_1 V_{r1} \end{bmatrix} \tag{48}$$

The pressure components:

$$P_r = -r \frac{\partial p}{\partial r} \begin{bmatrix} \alpha_1 C_{p1} \\ \alpha_2 C_{p2} \\ 0 \\ 0 \\ 0 \end{bmatrix} \tag{49}$$

The components of gG_r:

$$gG_r = \begin{Bmatrix} \alpha_1 \left[C_{11} \frac{\partial r\alpha_1\tau_{rr1}}{\partial r} + \alpha_1 C_{12} \frac{\partial r\alpha_2\tau_{rr2}}{\partial r}\right] \\ \alpha_2 \left[C_{21} \frac{\partial r\alpha_1\tau_{rr1}}{\partial r} + C_{22} \frac{\partial r\alpha_2\tau_{rr2}}{\partial r}\right] \\ \alpha_1 \left[C_{11} \frac{\partial r\alpha_1\tau_{r\theta 1}}{\partial r} + C_{12} \frac{\partial r\alpha_2\tau_{r\theta 2}}{\partial r}\right] \\ \alpha_2 \left[C_{21} \frac{\partial r\alpha_1\tau_{r\theta 1}}{\partial r} + C_{12} \frac{\partial r\alpha_2\tau_{r\theta 2}}{\partial r}\right] \\ 0 \end{Bmatrix} \tag{50}$$

and the components of S:

$$S = \begin{Bmatrix} \alpha_1 \left[V_{\theta 1}^2 + C_{d1} r (V_{r1} - V_{r2}) + \sum_{\ell=1}^{2} C_{1\ell} (\alpha_\ell \rho_\ell B_{r\ell} r - \alpha_\ell \tau_{\theta\theta\ell})\right] \\ \alpha_2 \left[V_{\theta 2}^2 + C_{d2} r (V_{r1} - V_{r2}) + \sum_{\ell=1}^{2} C_{2\ell} (\alpha_\ell \rho_\ell B_{r\ell} r - \alpha_\ell \tau_{\theta\theta\ell})\right] \\ \alpha_1 \left[-V_{r1} V_{\theta 1} + C_{d1} r (V_{\theta 1} - V_{\theta 2}) + \sum_{\ell=1}^{2} C_{1\ell} (\alpha_\ell \rho_\ell B_{\theta\ell} r - \alpha_\ell \tau_{r\theta\ell})\right] \\ \alpha_2 \left[-V_{r2} V_{\theta 2} + C_{d2} r (V_{\theta 1} - V_{\theta 2}) + \sum_{\ell=1}^{2} C_{2\ell} (\alpha_\ell \rho_\ell B_{\theta\ell} r - \alpha_\ell \tau_{r\theta\ell})\right] \\ 0 \end{Bmatrix} \tag{51}$$

All the components of F, P_r, gG_r and S can be regarded as functions of the components of W which are the independent variables.

3.5.2 Numerical Scheme

One way to solve equation (46) numerically is to solve the pressure field first from equation (22) then integrate equation (46) to obtain the solution at the new time step. To ensure an accurate result, the solution so obtained should be used as a check to satisfy both the continuity equations in addition to the phase definition of $\alpha_1 + \alpha_2 = 1$. In general, the continuity equations probably will not be satisfied by the solution due to the numerical approximation. Thus, an iteration on the pressure field or other treatment would be needed to attain a desirable accuracy.

Another numerical procedure that has been used very extensively [19] will be adopted here for our purposes. Basically, the procedure first solves the equations with no pressure terms, then adds the pressure correction back to the solution. Thus, from equation (46), we could have

$$\frac{W^* - W^n}{\Delta t} = F_r^n + gG_r^n + S^n \tag{52}$$

and

$$\frac{W^{n+1} - W^*}{\Delta t} = \hat{P}_r \tag{53}$$

where W* is the intermediate solution of W without pressure terms at the new time step n+1, the superscript n and n+1 denote the values at the initial time and the new time steps, respectively, and the elements of P_r have the similar format as those of equation (49), i.e.,

$$\hat{P}_r = -r \frac{\partial \hat{p}}{\partial r} \begin{bmatrix} \alpha_1 C_{p1} \\ \alpha_2 C_{p2} \\ 0 \\ 0 \\ 0 \end{bmatrix} \tag{54}$$

The overhead symbol ^ here indicates the corrected terms of the pressure field. This is used to distinguish the pressure from those of the regular time steps n or n+1.

From the continuity condition of equation (12), we have

$$\nabla \cdot \left[\left(\frac{W_1 + W_2}{r} \right) \bar{n}_r + \left(\frac{W_3 + W_4}{r} \right) \bar{n}_\theta \right] = 0 \tag{55}$$

for each time step. Substituting eqs. (54) and (55) into equation (53). We have the Poisson type equation for pressure field as

$$\nabla \cdot \left[(\alpha_1 C_{p1} + \alpha_2 C_{p2}) \nabla \hat{p} \right] \Delta t = \nabla \cdot \left[\left(\frac{W_1^* + W_2^*}{r} \right) \bar{r} + \left(\frac{W_3^* + W_4^*}{r} \right) \bar{\theta} \right] \tag{56}$$

Thus, the numerical procedure is: 1) to get W* by solving the system of equations (52) without the pressure gradient terms; 2) to get pressure gradient $\nabla \hat{p}$ by solving eq. (56); and 3) then to correct the solution by using equation (53).

For axisymmetric cases, equation (56) reduces to

$$\frac{\partial \hat{p}}{\partial r} = \frac{W_1^* + W_2^*}{(\alpha_1 C_{p1} + \alpha_2 C_{p2})\, r\Delta t} \tag{57}$$

and

$$\frac{\partial p}{\partial \theta} = 0$$

And the solution after the pressure correction is

$$W_1^{n+1} = -W_2^{n+1} = \frac{\alpha_2 C_{p2} W_1^* - \alpha_1 C_{p1} W_2^*}{\alpha_1 C_{p1} + \alpha_2 C_{p2}} \tag{58}$$

$$W_3^{n+1} = W_3^*,\ W_4^{n+1} = W_4^*,\ W_5^{n+1} = W_5^*.$$

The fundamental theory of the MacCormack's scheme is briefly given below.

For second order accuracy, the solution of eq. (46) could be written as

$$W^1 = W^o + \Delta t\, W_t^{\,o} + \frac{(\Delta t)^2}{2} W_{tt}^{\,o}$$

$$= W^o + \frac{\Delta t}{2} W_t^{\,o} + \frac{\Delta t}{2} (W_t^{\,o} + \Delta t\, W_{tt}^{\,o})$$

$$= \frac{1}{2} (W^o + \Delta t\, W_t^{\,o}) + \frac{1}{2} (W^o + \Delta t\, W_t^{\,p})$$

$$= \frac{1}{2} (W^p + W^c) \tag{59}$$

where

$W^p = W^o + \Delta t\, W_t^{\,o}$ is the predicted value,

and

$W^c = W^o + \Delta t\, W_t^{\,p}$ is the corrected value.

The superscripts denote the time-level of the information and subscripts denote the partial derivative with respect to either time t or space r. Specifically, superscripts 0 and 1 are the initial and the completely advanced time (here two steps) plane; p and c are the predicted (1st step) and corrected (2nd step) time plane. Thus, W_t^o is the time derivative of W evaluated at the initial time, and W_t^p is time derivative of W evaluated at the predicted time.

Fig. 10 shows the diagram of the two step difference scheme used in the computer program. Due to the difference scheme, the spatial location after each step in time is a half grid off from the original one. Thus, the spatial offset which resulted from a backward predicting step will cancel with those of the forward correcting step.

Numerically, the predicted values are

$$W_i^p = \frac{1}{2} (W_{i-1/2}^p + W_{i+1/2}^p) \tag{60}$$

where

$$W_{i-1/2}^p = \frac{1}{2} (W_{i-1}^o + W_i^o) + \Delta t\, W_t^o$$

$$= \frac{1}{2} (W_{i-1}^o + W_i^o) + \frac{\Delta t}{\Delta r} \left[(F_i^o - F_{i-1}^o) + \frac{(g_i^o + g_{i-1}^o)}{2} (G_i^o - G_{i-1}^o)\right]$$

$$+ \frac{\Delta t}{2} (S_i^o + S_{i-1}^o) + \Delta t\, \hat{P}_{i-1/2}^p \tag{61}$$

and the corrected value is evaluated at the predicted time place, that is at $W_{i+1/2}^p$. Thus

$$W_i^c = W_i^o + \Delta t\, W_t^p$$

$$= W_i^o + \frac{\Delta t}{\Delta r}\left[\left(F^p_{i+1/2} - F^p_{i-1/2}\right) + \frac{\left(g^p_{i+1/2} + g^p_{i-1/2}\right)}{2}\left(G^p_{i+1/2} - G^p_{i-1/2}\right)\right]$$

$$+ \frac{\Delta t}{2}\left(S^p_{i+1/2} + S^p_{i-1/2}\right) + \Delta t\, \hat{P}_i^c \qquad (62)$$

Here $\hat{P}^p_{i-1/2}$ and $\hat{P}_i^c$ are the pressure correction terms as discussed before (eq. 52-58). Thus, for each time step, the advance is carried out in two steps: a full step backward predictor, eq. (61) and then a forward corrector, eq. (62). As indicated in the diagram, the subscript i in the regular mesh spatial location at which solution is to be advanced, $i \pm 1$ is the spatial location of regular mesh points immediately to the right and left of the location i, $i \pm 1/2$ is the location midway between i and $i + 1$ or between $i - 1$ and i at the predictor plane. Thus, for each time step as the procedure advanced, the outermost data points at the boundary are not updated through the numerical scheme. The values at the boundary are to be given through some suitable boundary conditions. The numerical procedure utilizes a uniformly preselected spatial mesh and variable time increment. To avoid a singularity at the center of the core region, a finite radius R_i is used for the inner boundary. The tank radius R is the outer boundary. The time step is determined at each time step to ensure numerical stability [20]. For a finite grid size Δr, the maximum time step Δt is given by

$$\Delta t_k = 1/\left[\left|C_{dk}\right| + \left|V_{rk}\right|/\Delta r + \frac{2}{\Delta r^2}\left(\alpha_1 \mu_1^e C_{k1} + \alpha_2 \mu_2^e C_{k2}\right)\right] \qquad (63)$$

where k = 1 and 2. The minimum Δt_k (with some rounding off) is used for the time step. Normally, the technique with the time step condition of equation (63) gives fairly good numerical stability. However, in critical conditions numerical damping can be added either for damping oscillations due to large gradients or for accelerating the calculation by increasing the time step. A damping factor, D thus was added in the program as

$$W_i^{1D} = W_i^1 (1-D) + (W_{i-1}^1 + W_{i+1}^1 - W_i^1) D \qquad (64)$$

where W_i^1 is the value obtained based on the two-step scheme, and W^{1D} is the value after the damping factor D is added. A typical value of D is 0.2. All the examples presented in the following section are based on D=0. That is, no damping factor is used.

The computer program was written in a Fortran 77 based computer code. The code will permit evaluation of the effects of various parameters which control the fluid dynamical behavior. These include tank size, fluid properties, such as density and viscosity, etc., characteristic gas bubble and liquid drop sizes, and relative location of injection nozzles. Also, the program was developed and arranged in such way that different modelings can be easily adapted.

3.6 Numerical Results

The flexibility and ease of changing test conditions are the major advantages of a numerical test as opposed to an experimental test. The computer program is developed to accept various conditions and model parameters. Fluid properties, (ρ_k, μ_k), initial volume fraction distributions (α_1), initial velocity distributions, boundary and injection

conditions, Reynolds number and several modeling constants are among the input quantities. Various cases have been tested during the course of the program development. To limit the size of this report, only a few typical cases will be presented. The common conditions for all the test runs presented here are as follows:

1) Uniformly distributed initial volume fraction (initially, gas volume fraction = 0.25 everywhere).
2) Air/water case: $\rho_1/\rho_2 = 1.293 \times 10^{-3}$, $\mu_1/\mu_2 = 1.13 \times 10^{-2}$, $\rho_2 = 10^3$ kg/m^3, and $\mu_2 = 1.514 \times 10^{-3}$ kg/m-s.
3) Bubble/droplet size obeys the power law of $d_k = 0.01 \times \alpha_k^{0.2}$
4) Jet opening: $0.85 < r_j < 0.95$
5) Weighting powers for drag and added mass coefficients: $n_d = n_a = 4$
6) Characteristic Reynolds number, $Re = \rho_2 V_s R/\mu_2 = 10^5$
7) Length scale = tank radius R = 1 meter, Velocity scale = 0.1514 m/s, Time scale = 6.605 s, and Pressure scale = 22.922 P_a.

The other test conditions are summarized in Table I. These test runs assume either an initially pure rotational flow (linear swirl velocity distribution) or that the fluid is initially at rest. The initial angular rotation speed is ω (radians per unit time). The averaged mean injection speed across the jet opening is V_j. To specify the boundary condition at the tank wall, I_w is used - with $I_w = 1$ being a non-slip condition and $I_w = 0$ being a free surface condition with no shearing forces. In either case, there is no radial velocity at the wall boundary. In addition, I_w is also used to modify the initial velocity condition near the wall. For $I_w = 1$, a factor of $(1 - r)^{0.1}$ was included on the initial tangential velocity field when a simple vortex flow is assumed. This is assumed to simulate the power law velocity distribution near the wall. To avoid the effects of numerical

Test Run No.	I.C.	B.C. I_w	Injection Speed, V_j	μ_1^t/μ_1	μ_2^t/μ_2
148	$\omega = 1$	1	0	115	1000
149	$\omega = 1$	1	0	1000	1000
150	$\omega = 1$	0	0	115	1000
151	at rest	1	10, $(t \leq 3)$ 0, $(t > 3)$	115	1000
152	at rest	1	10, $(t > 0)$	115	1000
153	at rest	1	10, $(t > 0)$	1000	1000
154	at rest	1	5, $(t > 0)$	115	1000

For all the above cases the following conditions prevail: 1) Uniformly distributed initial gas volume fraction of $\alpha_1 = 0.25$; 2) $\rho_1/\rho_2 = 1.293 \times 10^{-3}$, $\mu_1/\mu_2 = 1.13 \times 10^{-2}$; 3) Bubble/droplet size obeys $d_k = 0.001 \times \alpha_k^{0.2}$; 4) Jet opening: $0.85 < r_j < 0.95$; 5) $n_a = n_d = 4$; 6) $Re = 10^5$; 7) Air-water fluids ($\rho_2 = 10^3$ kg/m^3, $\mu_2 = 1.514 \times 10^{-3}$ kg/m-s), Length scale = tank radius = 1 meter, velocity scale $V_s = 0.1514$ m/s, Time scale = 6.605 s, and pressure scale = 22.922 P_a.

Table I. Conditions of Test Runs.

singularities at the origin, a finite center core region was excluded from the analysis. For the data presented here the inner radius is 10% of the tank radius. At this inner boundary, the free surface with no shearing forces is assumed at all times. The eddy viscosity factor is μ_k^t/μ_k. For liquid phase, $\mu_2^t/\mu_2 = 1000$ was assumed for all cases, while two values of μ_1^t/μ_1 were tested for gas phases. The value of $\mu_1^t/\mu_1 = 115$ corresponds to the condition of the same kinematic eddy viscosity for both phases (i.e., $\nu_1^t = \nu_2^t$). This is based on the expression of the eddy stress that $\rho vv \approx \mu^t \nabla V$. As discussed by Drew [6], if both phases have similar velocity fields, the kinematic eddy viscosities ($\nu_k^t = \mu_k^t/\rho_k$) representing both velocity scales and mixing lengths of large eddy processes should be approximately equal. If this is the case, then the eddy viscosity factor $\mu_1^t/\mu_1 = (\nu_2/\nu_1)(\mu_2^t/\mu_2)$. For air water case, if $\mu_2^t/\mu_2 = 1000$, then $\mu_1^t/\mu_1 \approx 115$.

Thus, as shown on Table I, test runs 148 to 150 are for an initially pure rotational flow with no flow injection. Test runs 151 to 154 begin with the fluid at rest initially but with flow injection. Although the initially pure rotational flow cannot exist in reality, it is a good way to test the essential physical mechanisms of vortex-induced, phase-separation. On the other hand, the vortex flow induced by the flow injection of tests 151 to 154 are good simulations to the actual situation. These spin-up tests are thus good examples to study the fluid dynamical behavior of the two-phase fluids in the sender tank.

Figs. 11 to 15 show the velocity vector distributions for various test runs. The test results for #149 and #154 are not shown here because the result of #149 is practically identical to that of #148, and that of #154 is very similar to that of #152. In these figures, Fig. (a) shows the gas phase and Fig. (b) shows the liquid phase. At this point, it should be

noted that the actual flow fields are all axisymmetric and the angular coordinate replaced by the temporal variation in the displays is done only for ease of observation. To produce these displays, the radial distributions at the different times are oriented along equally-spaced angles. This angular separation arrangement should not be interpreted as an angular variation in the flow field for the results.

In Figs. (13), (14) and (15), the region of injection is shown in the annular region between two dashed circles.

These velocity vector fields indicate all flows are primary in angular rotation with gas phase tending to move inward and liquid phase trying to move outward, as expected. Since the wall shear stress will slow the flow movement, the vortex flow will diminish eventually if there is no injection introduced, as Figs. (11) and (13) indicate. The effect of eddy viscosity factor can also be seen from Figs. (14) and (15). Fig. 15 shows the velocity distribution is more uniform and extends more into the center region than that of Fig. 14. This is due to the larger gas eddy viscosity factor, μ_1^t/μ_1 on #153 than on #152. Since the main mechanism to establish a flow rotation outside the region of injection is the shearing stress distribution that results from the finite effective viscosity flow having larger eddy viscosity should transfer and diffuse the locally injected momentum more effectively. Although the effect of eddy viscosity can be found in the injection cases, it shows practically no difference between cases of #148 and #149. This is because in these cases, the flows are already in pure rotation and thus the transfer or diffusion of the momentum is not very important.

Figs. 16(a),(b),(c) and (d) show more details of the velocity distributions of the test #148. To keep the figure clear, most of the

following figures will show only the data at six times, t = 0,1,2,3,4, and 5. The tangential velocities shown in Figs. 16(a) and (b) for gas and liquid phases respectively are decreasing in time due to the wall stress. Figs. 16(c) and (d) show the corresponding radial velocities. They indicate the gas phase has negative radial velocity and the liquid phase has positive radial velocity. That is, gas is moving inwardly and liquid is moving outwardly. Also, except near t = 0, the strength of these movements is decreasing. This decrease is mainly due to the decreasing of the tangential velocity. Near t = 0, the radial velocity is accelerating since the analysis starts with no radial velocity.

As the result of these radial movements, the volume fraction distribution is also changed with time. Fig. 17 shows the gas volume fraction distributions of test #148 as functions of time. As expected, the gas volume fraction is increasing at the inner region and decreasing at the outer region. However, because of the decaying vortex as the result of the wall stresses, the minimum gas volume fraction can only reach about 0.18 even near the wall. That is, for this case a complete separation between gas and liquid phases seems to be impossible. Fig. 18 shows the gas volume fraction distributions of test #150 as functions of time. Since a free surface, ($I_w = 0$) was assumed for this case, the vortex strength remains nearly constant. As the result of the constant rotational strength, the radial movements continue and the gas volume fraction approaches zero near the wall. That is, there is a liquid layer formed near the wall region for this case.

Fig. 19(a) shows the liquid tangential velocity of test #152. Near the region of injection ($0.85 < r < 0.95$), the tangential velocity is increasing from zero very quickly at first and then approaching an asymptotic value.

Meanwhile the angular momentum (or the tangential velocity) is transferred and diffused into the inner region. Fig. 19(b) shows the liquid radial velocity of the same test. Although the maximum tangential velocity always appears near r = 0.85, the location of the maximum radial velocity continues to move inwardly. This can be explained more easily from the time evolution of the volume fraction distributions as shown in Fig. 20. Except t = 0, there is an annular layer formed near the wall, in which the gas volume fraction is zero. This annular liquid layer grows with time, and the interfacial radius of this layer is moving inwardly. Since a liquid layer contains little or no gas, the associated radial movement will be very small even if the flow has a large angular rotation. Therefore, the location of the maximum radial velocity is moving inwardly despite the fact that the location of the maximum tangential velocity remains nearly unchanged at r = 0.85.

For comparison, the liquid velocity distributions of test #151 for t = 4 and 5 are also shown on Figs. 19(a) and (b). The conditions for #151 are same as those of #152 except the injection rate is shut off after t = 3. Thus for t < 3, all the data are exactly the same as those of #152. Due to the effect of the viscosity, the peak momentum will continue to diffuse and transfer to the region of lower momentum, particularly at the wall where a momentum sink is located. Figs. 19(a) and (b) show that both the tangential and radial components of the velocity are decreasing with time as the injection is turned off at t = 3. However, the decrease of the tangential velocities is much larger than that of the radial component. Fig. 20 also shows the gas volume fraction distributions of #151. Even the velocity fields are quite different between cases #151 and #152 especially for the tangential component. The volume fraction distributions between these two

cases are practically the same. This indicates the final part of the injection (i.e., $t > 3$) is very ineffective.

Fig. 21 shows the gas volume fraction distributions of test #153. This shows that a larger gas eddy viscosity can produce a better separation, especially for the region far away from the region of the injection. Fig. 22 shows the gas volume fraction distributions of test #154. As expected, lower injection speed will produce smaller phase separation. However, the effect is not linear. From Figs. (20) and (22) the time required to produce a liquid layer of 15% of radius, is about 1 for #152 and about 3 for #154. That is, a factor of 2 reduction on the injection speed will require a factor of 3 increase on time.

To study fluid dynamical behavior of these two-phase fluids, it is useful to know the velocity fields. To design a practical tank system, it is important to know the pressure distribution in the tank. Figs. (23) and (24) show the pressure distributions of tests #148 and #152, respectively. The pressure distributions of test #151 at $t = 4$ and 5 are also shown in Fig. 24 for comparison.

As expected the data show the maximum pressure occurs at the tank wall for all cases. For the case of initially pure rotation (#148), the pressure field is decreasing as the rotational speed reduces. The slightly different character that appears in the pressure distribution at $t = 0$ is due to the assumption of no initial radial velocity. The initial pressure field essentially is that of the centrifugal forces due to the pure rotation. As time goes by, the radial velocity increases and the pressure field is thus adjusted accordingly. In the injection cases, the pressure field gradually increases as the injection continues. As soon as the injection is stopped, the pressure field is changes as shown by #151 in Fig. 24.

As discussed earlier regarding the operation concept, the time evolution of vortex strength and the degree of phase separation are the important operation parameters. The definitions of these parameters are arbitrary and depend on various situations or requirements. Some of these quantities are defined below:

a) Vortex Strength Γ, the total angular momentum per unit volume:

$$\Gamma = \sum_{i=1}^{2} \overline{\alpha_i \rho_i V_{\theta i} r} = \sum_{i=1}^{2} \rho_i \frac{\int \alpha_i V_{\theta i} r^2 dr}{(R^2 - R_1^2)}$$

b) Separation Strength $\bar{Q}_r$, the averaged radial flow rate per unit volume:

$$\bar{Q}_r = \frac{\int 2\pi r \alpha_2 V_{r2} dr}{\pi(R^2 - R_1^2) \int dr} = \frac{2 \int \alpha_2 V_{r2} r dr}{(R^2 - R^1)(R - R_1)}$$

This indicates the rapidity with which the liquid phase moves to the wall region and the gas phase moves to the inner region of the circular tank. Thus a larger $\bar{Q}_r$ means a fast phase separation.

c) Liquid Purity, $\bar{\alpha}_2 (r_1, r_2)$, the averaged liquid volume fraction between the radii of r_1 and r_2:

$$\bar{\alpha}_2 (r_1, r_2) = \frac{2 \int_{r_1}^{r_2} \alpha_2 r dr}{(r_2^2 - r_1^2)}$$

For the data presented below, $r_1 = 0.8$ and $r_2 = 1$ are chosen. This is the region where the withdrawal port will most likely be located.

d) Separation Index, SPI.

$$SPI = \frac{\bar{R}_2 - \bar{R}_1}{\bar{R}_{2s} - \bar{R}_{1s}}$$

where

$$\bar{R}_k = \frac{\int \alpha_k r dA}{\int \alpha_k dA}$$

is the center of gravity of phase k, and $\bar{R}_{ks}$ is the center of gravity of phase k when the two phases are completely separated.

When two phases are completely separated, the liquid forms an annulus against the wall of the tank around a core of gas with a contact radius of

$$R_c = (R^2 - 2 \int \alpha_2 r dr)^{1/2}.$$

Thus

$$\bar{R}_{1s} = 2/3 \, (R_c^3 - R_1^3)/(R_c^2 - R_1^2)$$

$$\bar{R}_{2s} = 2/3 \, (R^3 - R_c^3)/(R^2 - R_c^2)$$

Thus, SIP = 0 indicates that the two phases are uniformly mixed together, SPI = 1 means two phases are completely separated, and SPI < 0 means more gas is in the outer region than in the inner region.

e) Mixing Index, MXI

$$MXI = \frac{\overline{\alpha_1 \alpha_2}}{\bar{\alpha}_1 \bar{\alpha}_2} = \frac{A \int \alpha_1 \alpha_2 \, dA}{[\int \alpha_1 dA][\int \alpha_2 dA]}$$

This is another quantity to identify the degree of separation. When mixing index equal to 1 (MXI = 1) it means two phases are completely mixed and the

volume fractions are uniformly distributed. When mixing index decreases to 0 (MXI = 0) it means there is no mixing between the two or they are separated completely.

Thus, some of the fluid dynamical behavior of the two phase fluids in the tank can be identified. These are the vortex strength Γ, the separation strength $\bar{Q}_r$, the liquid purity $\bar{\alpha}_2(0.8, 1)$, the separation index SPI, and the mixing index MXI. These are plotted versus time for various tests as shown on Figs. (25)-(29). In order to present these using the same ordinate scale, the quantity $50\bar{Q}_r$ (rather than $\bar{Q}_r$) was plotted. For test #148, Fig. 25 shows that the vortex strength is decreasing, and the separation strength reaches a maximum at $t \approx 0.5$ and then decreases monotonically. It also shows both liquid purity $\bar{\alpha}_2$ (0.8, 1) and separation index SPI are continuing to improve even though the vortex strength is decreasing. However, because the separation strength is small and decreasing, the mixing index maintains a very high value ($\sim$ 1) and the two phases are still mixed very well even at $t = 5$. (MXI $\approx$ 0.95 and SPI $\approx$ 0.27 at $t = 5$).

If the effect of the wall stress is removed as shown in test #150, the situation is somewhat different. Fig. 26 indicates the vortex strength remains nearly unchanged. Liquid purity $\bar{\alpha}_2$ (0.8, 1), separation strength $\bar{Q}_r$ and separation index, SPI are all improved much more as compared to Fig. 25. Although the two phases are not completely separated as indicated by both the values of SPI and MXI, the liquid purity $\bar{\alpha}_2$ has nearly reached the value of 1 when $t > 4$. This suggests that, even when the two phases are not completely separated, the liquid transfer could be started provided the withdrawal port is located near the wall. Fig. 27 shows the same quantities

for tests #152. For $t > 3$, the values for test #151 are also shown on the same figure. The figure shows there is little or no difference on the degree of separation between tests #151 and #152, although the corresponding vortex strengths are quite different for $t > 3$. This indicates again that the continuation of the injection of #152 for $t > 3$ is not very effective.

Fig. 28 shows the results of test #153. As compared to Fig. 27, the larger eddy viscosity factor improves the degree of separation. This is partly due to the more effective injection as the result of the larger diffusion of the injected angular momentum produced by the larger effective viscosity. Despite a better degree of separation, the values of $\bar{\alpha}_2$ (0.8, 1) are practically the same. That is, the eddy viscosity does not noticeably affect the flow dynamics in the region of $0.8 < r < 1$ near which the injection was made. The value of $\bar{\alpha}_2$ (0.8, 1) indicates the liquid layer at the tank wall reaches 20% of radii thick at $t = 1$ for both cases.

Fig. 29 shows the degree of phase separation for the lower injection case, test #154. As expected, the degree of phase separation increases slower than in the higher injection cases. Nevertheless, liquid purity $\bar{\alpha}_2$ (0.8, 1) reaches 1 at t 3 as opposed to at $t \approx 1$ for the higher injection cases.

3.7 Conclusions

A vortex-induced, liquid handling process adapted to two-phase fluids in zero gravity has been analyzed for a selected range of fluid and flow parameters. This transfer process has been divided in two stages: the initial "spin-up" stage and the liquid pump-out stage. The initial spin-up stage is modeled in the circular tank via tangential injection techniques.

The model is based on a two-phase, two-fluid continuum and it incorporates several interactions between phases - namely fluid drag and pertinent virtual mass. The model provides a mathematical framework containing the essential physical mechanisms on vortex-induced phase separation.

A computer program using a FORTRAN 77 based computer code and HP-1000 minicomputer was developed. The program is flexible and accepts various input parameters for different flow conditions. It can also be modified easily to include additional interaction effects. This program can be used to study the fluid dynamical behavior of two-phase fluids in the sender tank. It provides a quick/easy sensitivity test on various parameters and thus provides the guidance for the design and use of actual physical systems for handling two-phase fluids in space.

Several examples are given to demonstrate the products of the program. The interesting and plausible results seem to indicate the simplified two-phase two-fluid model is a useful one. However, detailed evaluation of the result is only possible with the aid of accurate local measurements. It is therefore concluded that this model should receive further attention in the form of experimental verifications. These verifications should be devised to check both the formulations selected for phase interactions as well as the results predicted.

Acknowledgments

We would gratefully acknowledge the support received from NASA's Kennedy Space Center to carry out the model-development work described herein. Specific thanks go to Mr. Frank Howard whose involvements and inputs on this project have been most helpful. We would also like to thank Drs. James M. McMichael and L. Patrick Purtell for their invaluable

contributions on the initiation and the early stage of this project. In addition, thanks are extended to Dr. George E. Mattingly for his encouragement and technical discussions; to Mr. Mike Hiza for his involvement on the project initiation; and to Ms. Susan Johnson for typing the manuscript.

References

1. Stark, J. A. (1976) "Low-G Fluid Transfer Technology Study", NASA CR-135020.
2. Wallis, G. B. (1982) "Review - Theoretical Models of Gas-Liquid Flows", ASME J. Fluid Eng. 104, 279.
3. Biesheuvel, A. and Van Wijngaarden, L. (1984) "Two-Phase Flow Equations for a Dilute Dispersion of Gas Bubbles in Liquid", J. Fluid Mech. Vol. 148, 301-318.
4. Delhaye, J. M. (1981) "Basic Equations for Two-Phase Flow Modeling", Two-Phase Flow and Heat Transfer in the Power and Process Industries, Bergles, A. E. et al., Eds., Hemisphere Publishing Corporation & McGraw-Hill Book Company, Chapter 2, 40-97.
5. Dobran, F. (1985) "Theory of Multiphase Mixtures", Int. J. Multiphase Flow, Vol. 11, no. 1, 1-30.
6. Drew, D. A. (1983) "Mathematical Modeling of Two-Phase Flow", Annual Review of Fluid Mechanics, Vol. 15.
7. Van Deemter, J. J. and Van Der Laan, E. T. (1960) "Momentum and Energy Balances for Dispersed Two-Phase Flow", Appl. Sci. Res., Sec. A, Vol. 10, 102-108.
8. Yadigaroglu, G. and Lahey, R. T. (1976) "On the Various Forms of the Conservation Equations in Two-Phase Flow", Int. J. Multiphase Flow, Vol. 2, 477-494.
9. Zuber, N. (1964) "On the Dispersed Two-Phase Flow in the Laminar Flow Regime", Chem. Eng. Sci., 19, 897.
10. Van Der Welle, R. (1981) "Turbulence Viscosity in Vertical Adiabatic Gas-Liquid Flow", Int. J. Multiphase Flow, Vol. 7, pp. 461-473.

11. Brenner, H. (1961) "The Oseen Resistance of a Particle of Arbitrary Shape", J. Fluid Mech. 11, 604.

12. Cook, T. L. and Harlow, F. H. (1984) "Virtual Mass in Multiphase Flow" Int. J. Multiphase Flow, Vol. 10, No. 6, 691.

13. Frankel, N. A. and Acrivos, A. (1967) "On the Viscosity of a Concentrated Suspension of Solid Spheres", Chem. Eng. Sci., 22, 847.

14. Ishii, M. and Zuber, N. (1979) "Drag Coefficient and Relative Velocity in Bubbly, Droplet or Particulate Flows", AIChE J. 25, pp. 843-55.

15. Lee, N. and Dukler, A. E. (1981) "A Stochastic Model for Turbulent Diffusion of Particles or Drops" AIChE J. Vol. 27, No. 4, 552.

16. Magnus, R. J. (1966) "Analytic Prediction of Pressure Pulses Due to the Rocket Engine Starting", General Dynamics, GDC-ERR-AN-984.

17. MacCormack, R. W. (1969) "The Effect of Viscosity in Hypervelocity Impact Cratering", AIAA Paper 69-354.

18. Chima, R. V. and Johnson, G. M. (1985) "Efficient Solution of the Euler and Navier-Stokes Equations with a Vectorized Multiple-Grid Algorithm", AIAA Vol. 23, No. 1.

19. Davis, R. W. (1983) "Finite Difference Methods for Fluid Flow", Proceedings of the 1983 International Conference on Computational Techniques and Applications", edited by John Noye and Clive Fletcher, pp. 51-69.

20. Peyret, R. and Taylor, T. D. (1983) "Computational Methods for Fluid Flow" Springer-Verlag, New York.

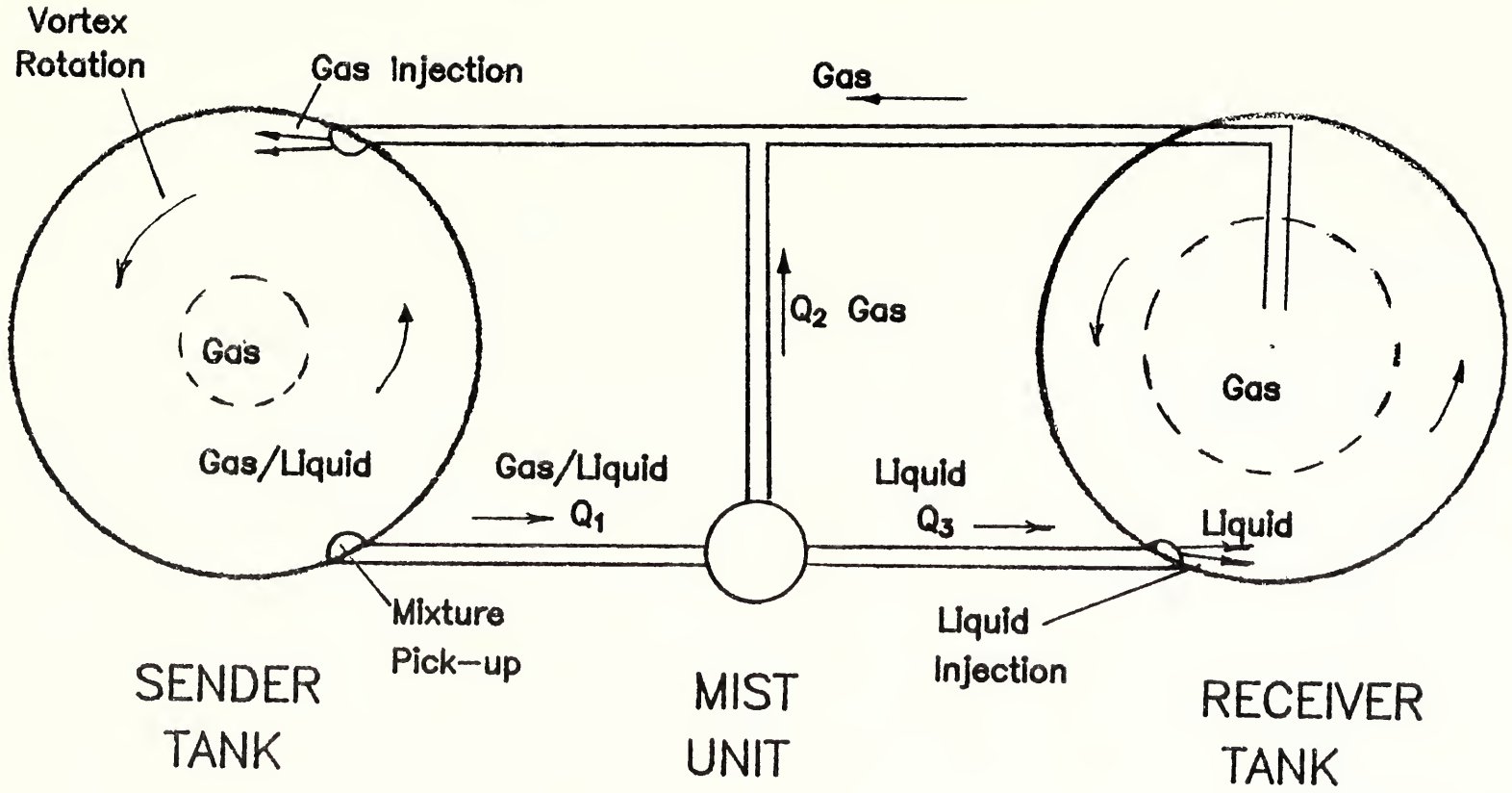

Figure 1. MIST Transfer System

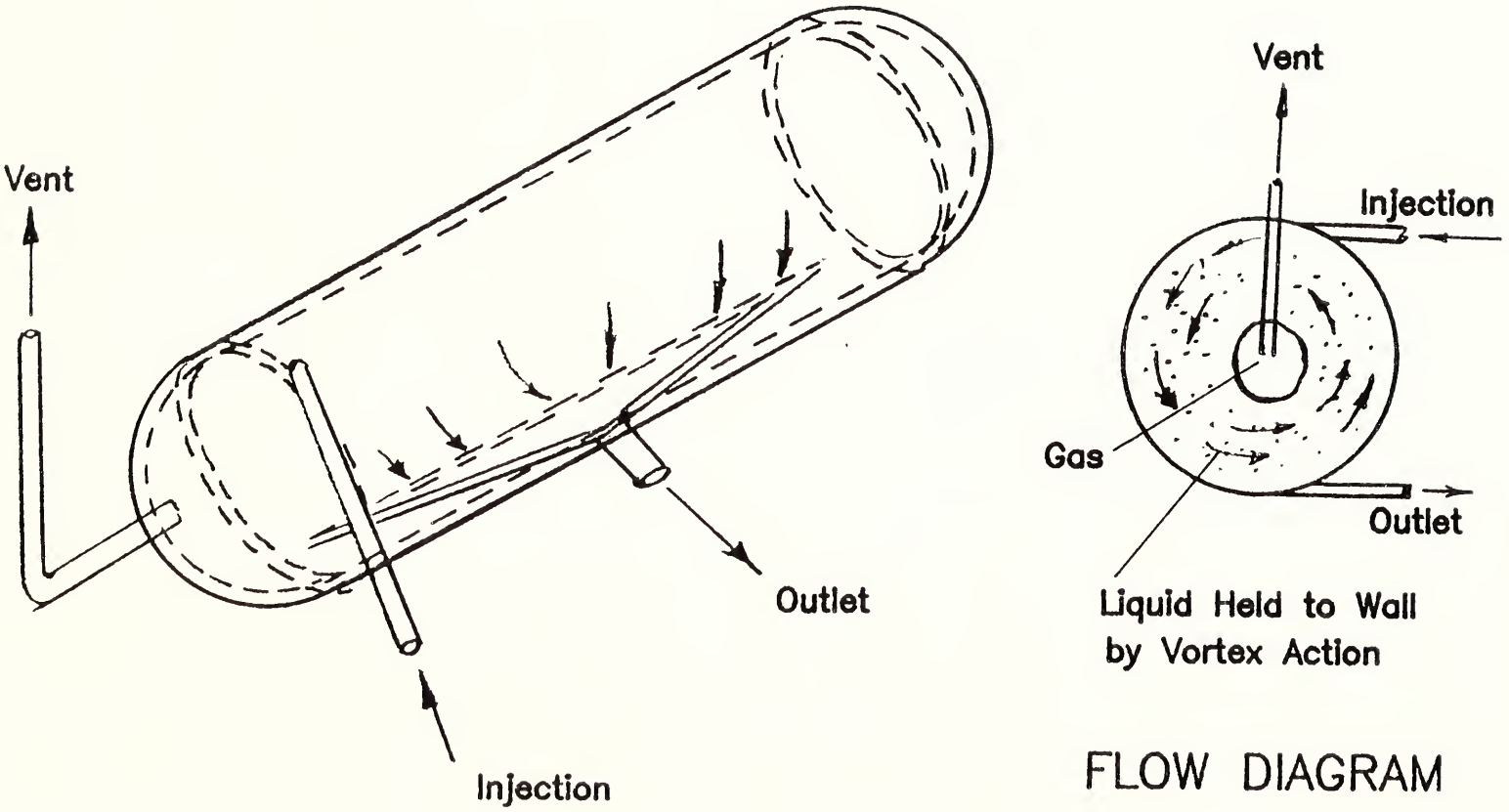

Figure 2. Tangential Vortex Model

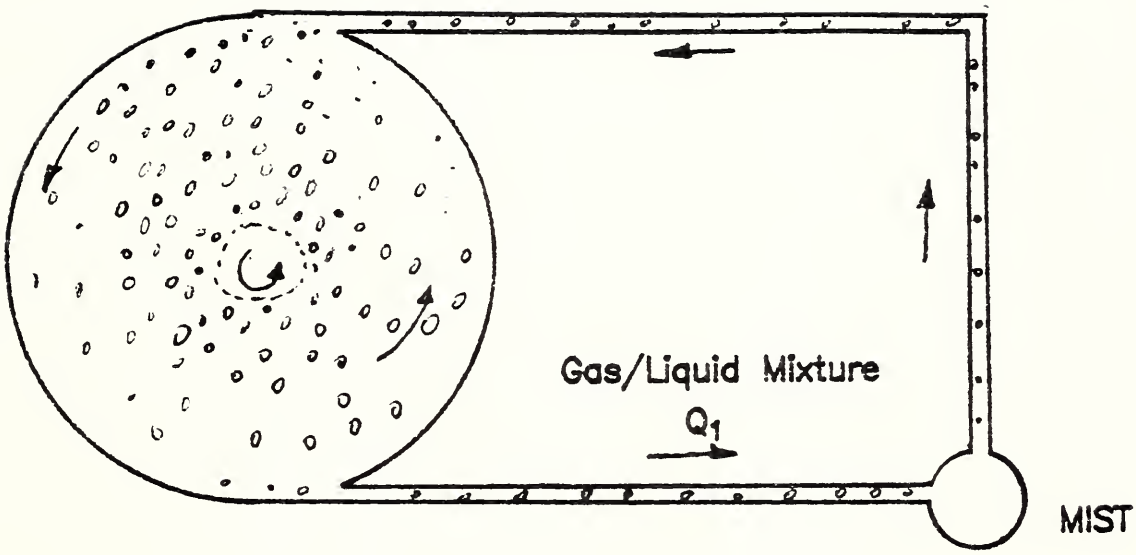

Figure 3. Start-up Configuration

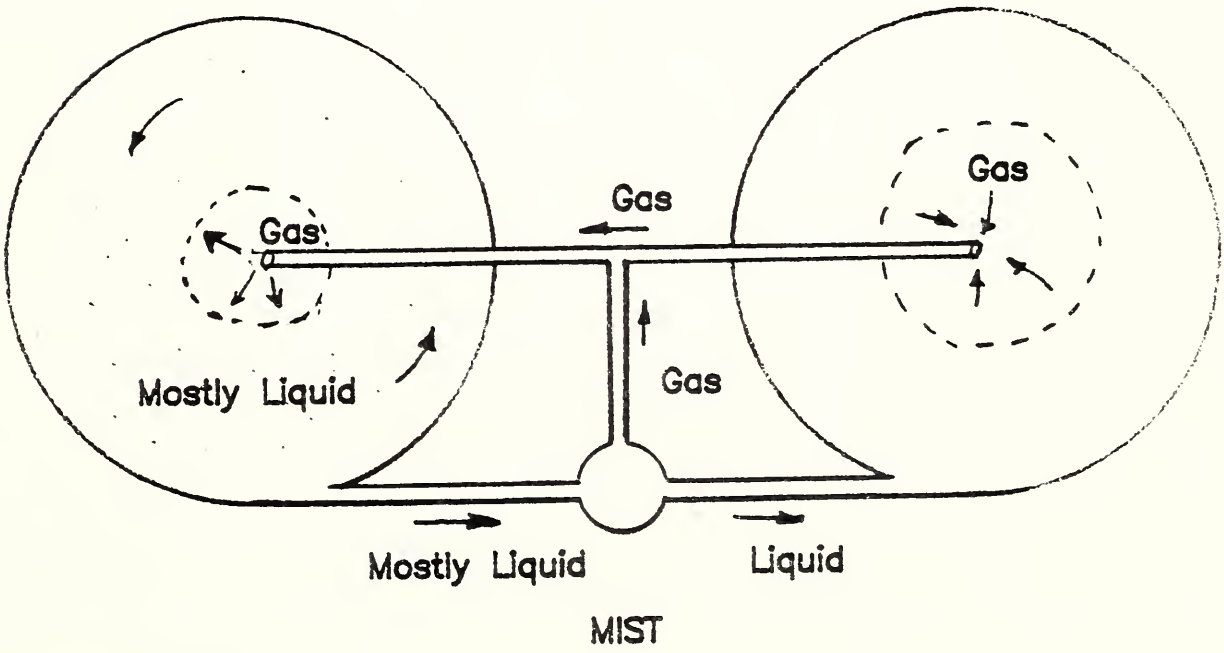

Figure 4. Pump-out Configuration

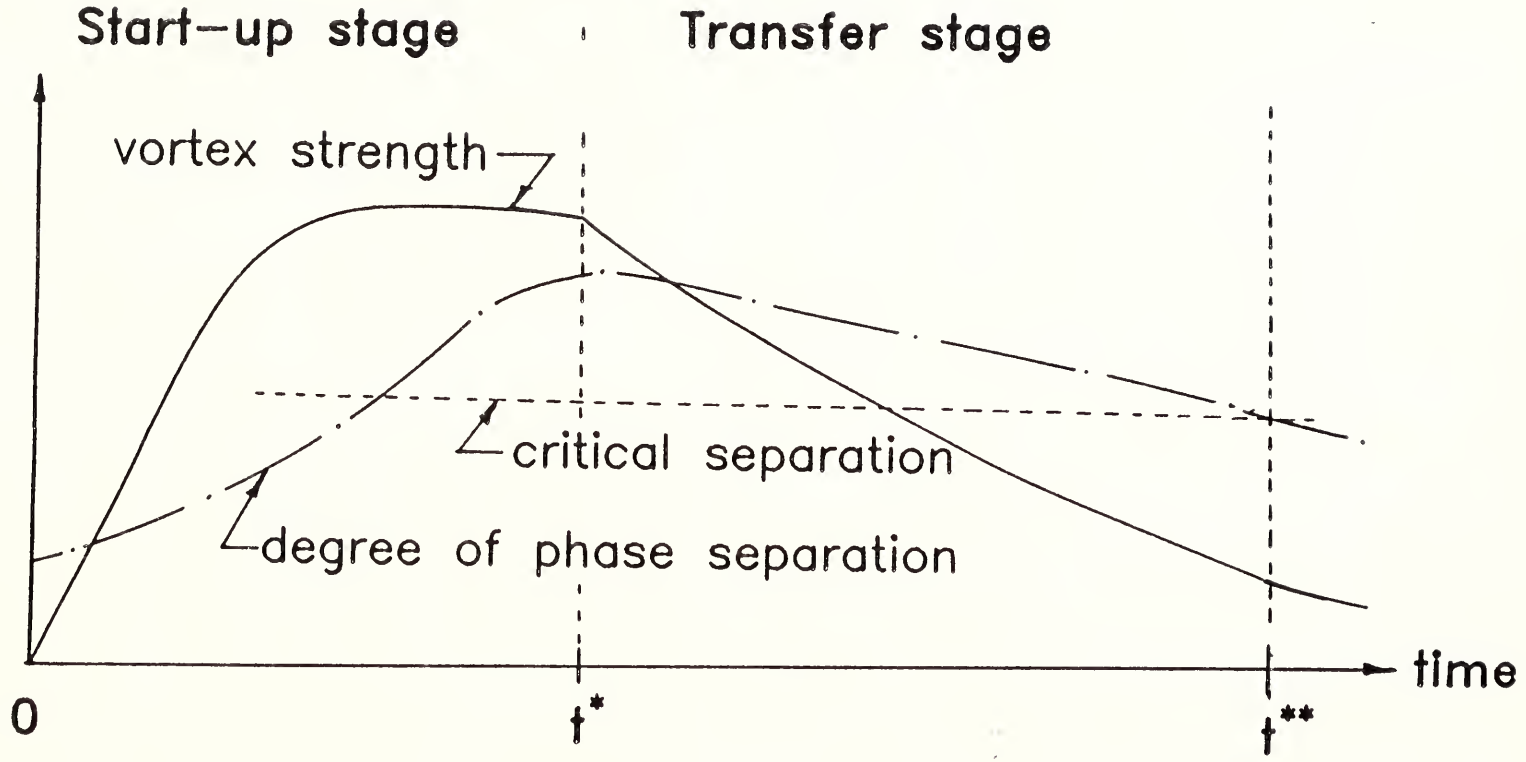

Figure 5. The Two-Stage Spin-up and Transfer Concept

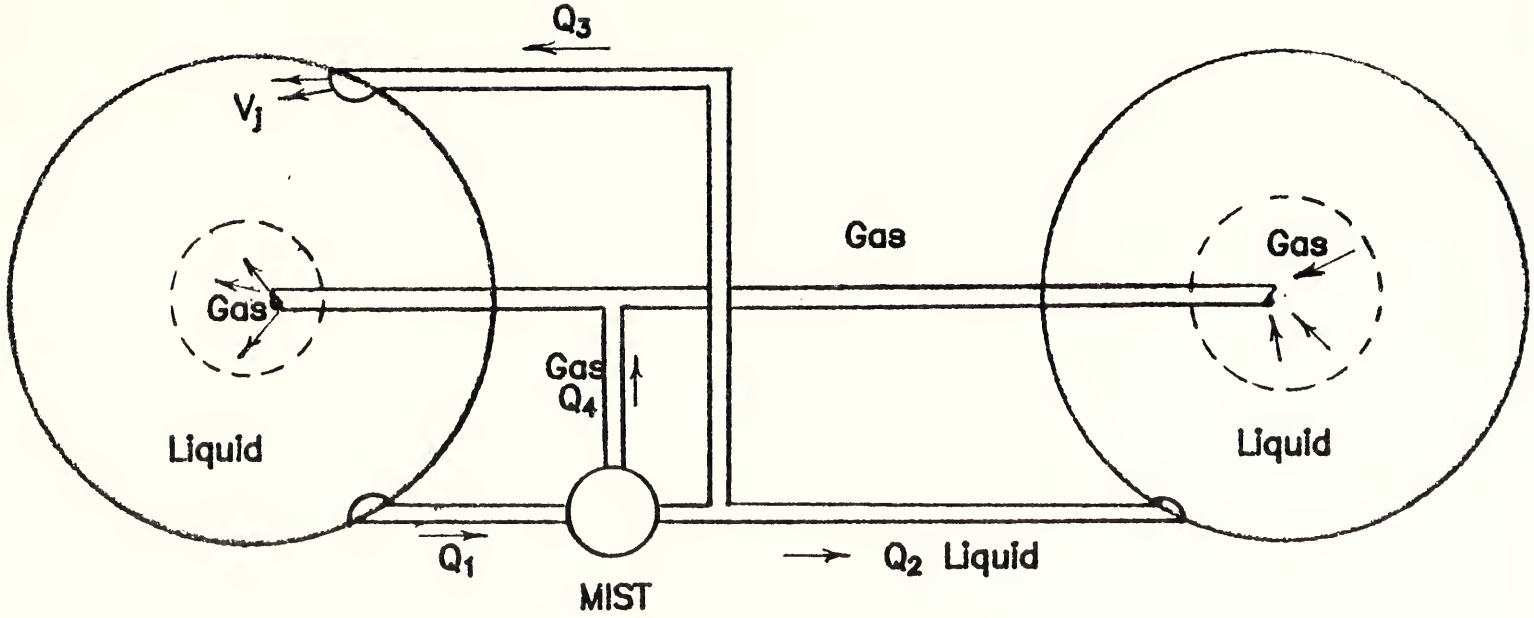

Figure 6. Modified MIST Transfer System
(Start-up stage: $Q_1 = Q_3$, $Q_2 = Q_4 = 0$
Pump-out stage: $Q_1 \simeq Q_2$, $Q_3 \simeq Q_4 \simeq 0$)

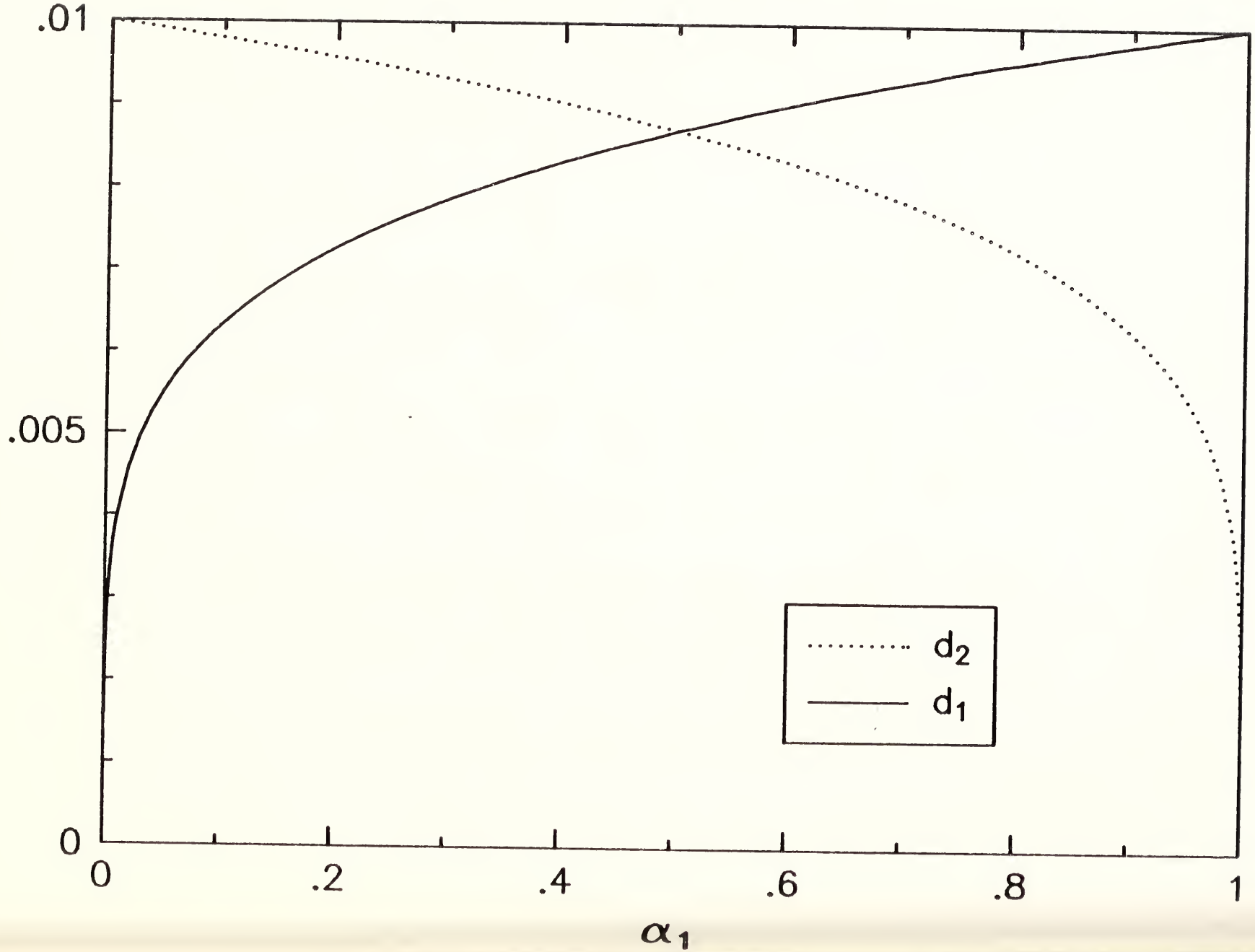
.01
.005
0
0
.2
.4
.6
.8
1
α_1
d_2
d_1

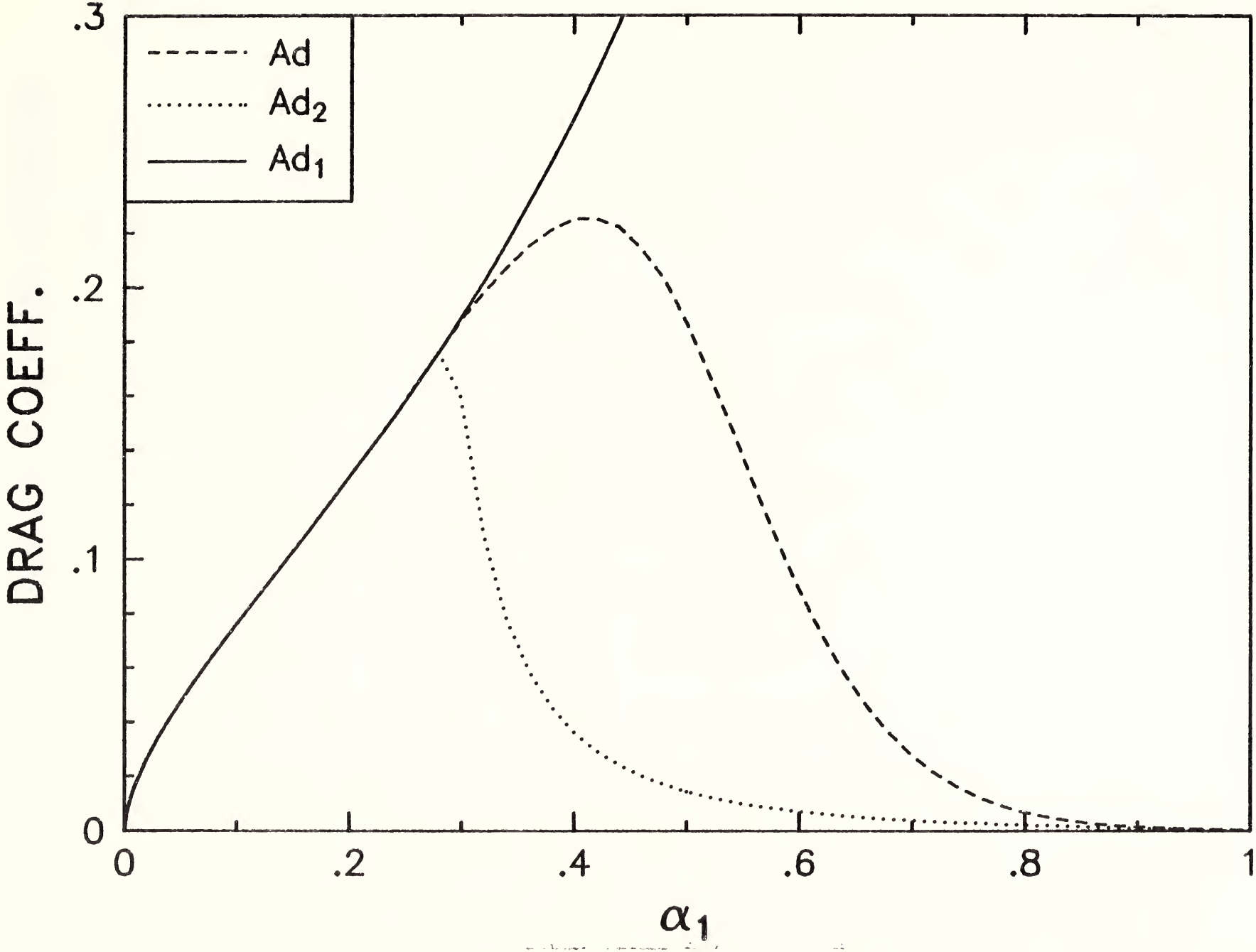

Figure 8. Modeling of Drag Coefficient

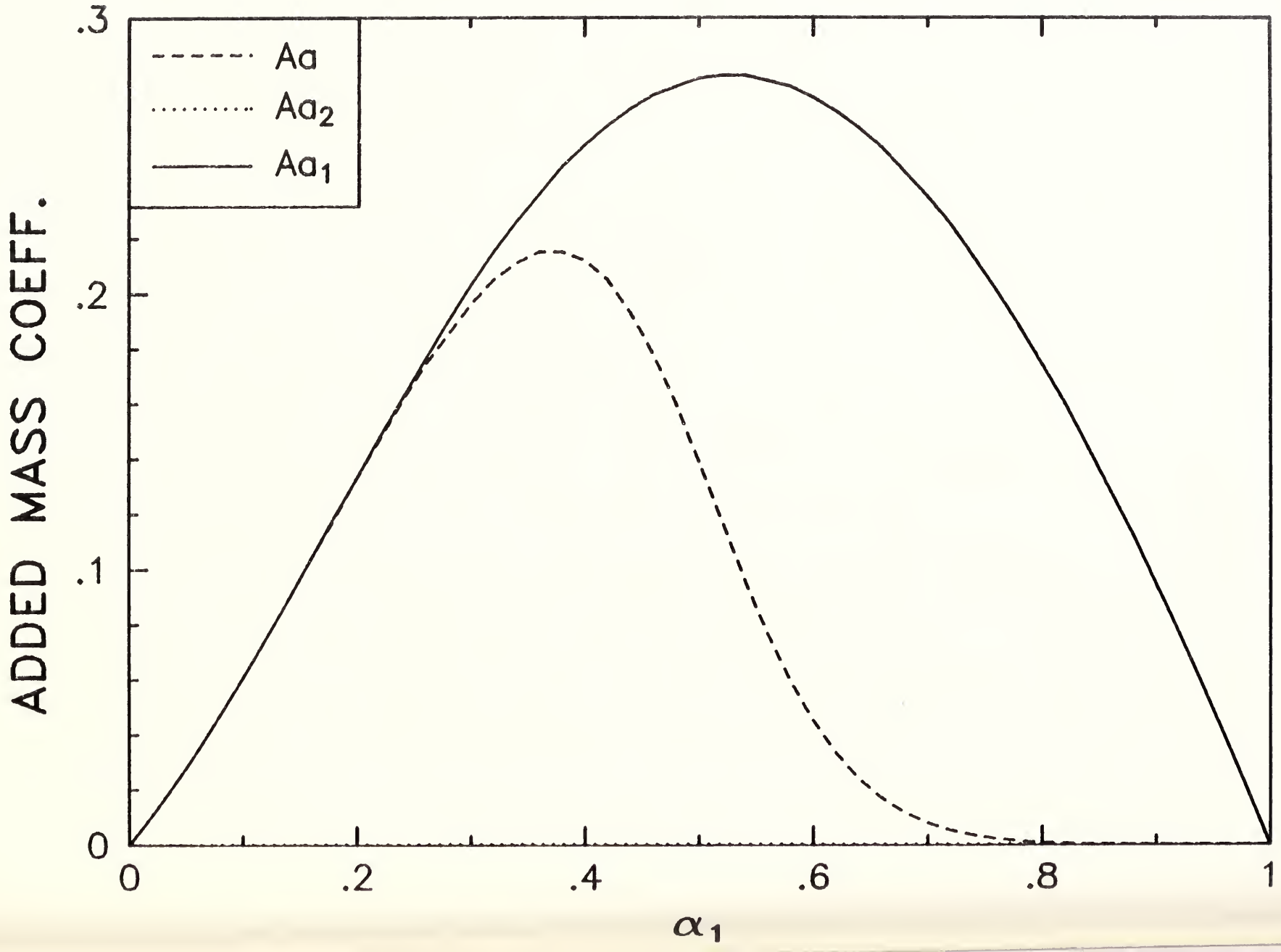
Aa
Aa2
Aa1
ADDED MASS COEFF.
.3
.2
.1
0
0
.2
.4
.6
.8
1
α1

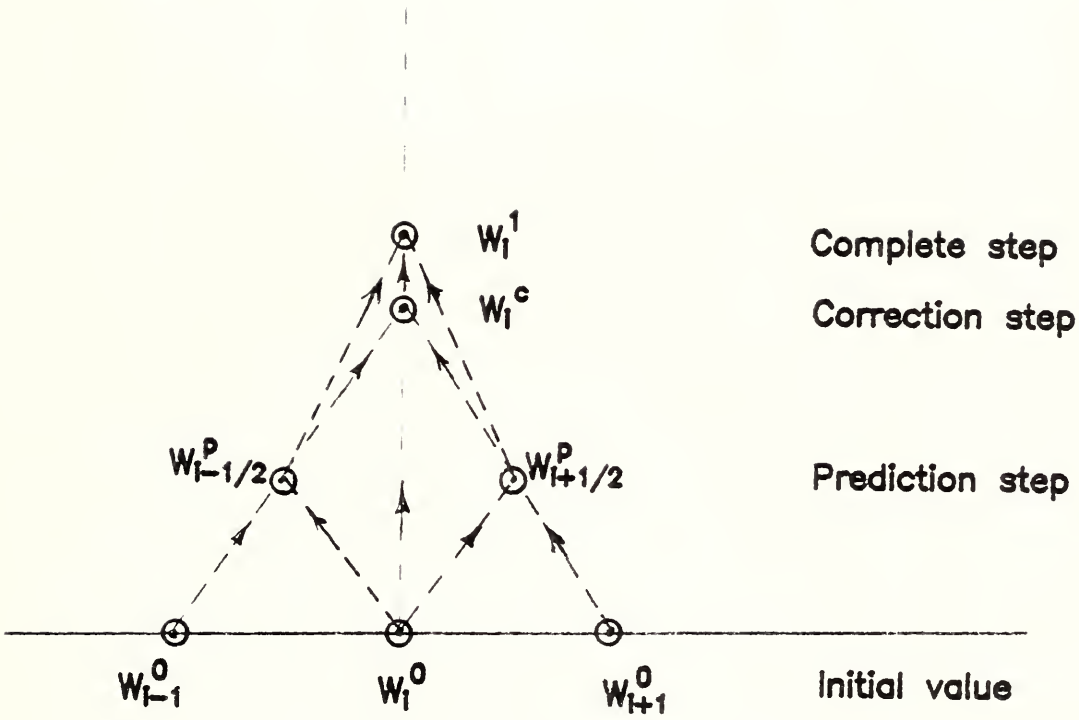

Figure 10. Two Step Difference Scheme (Backward Predictor - Forward Corrector Version)

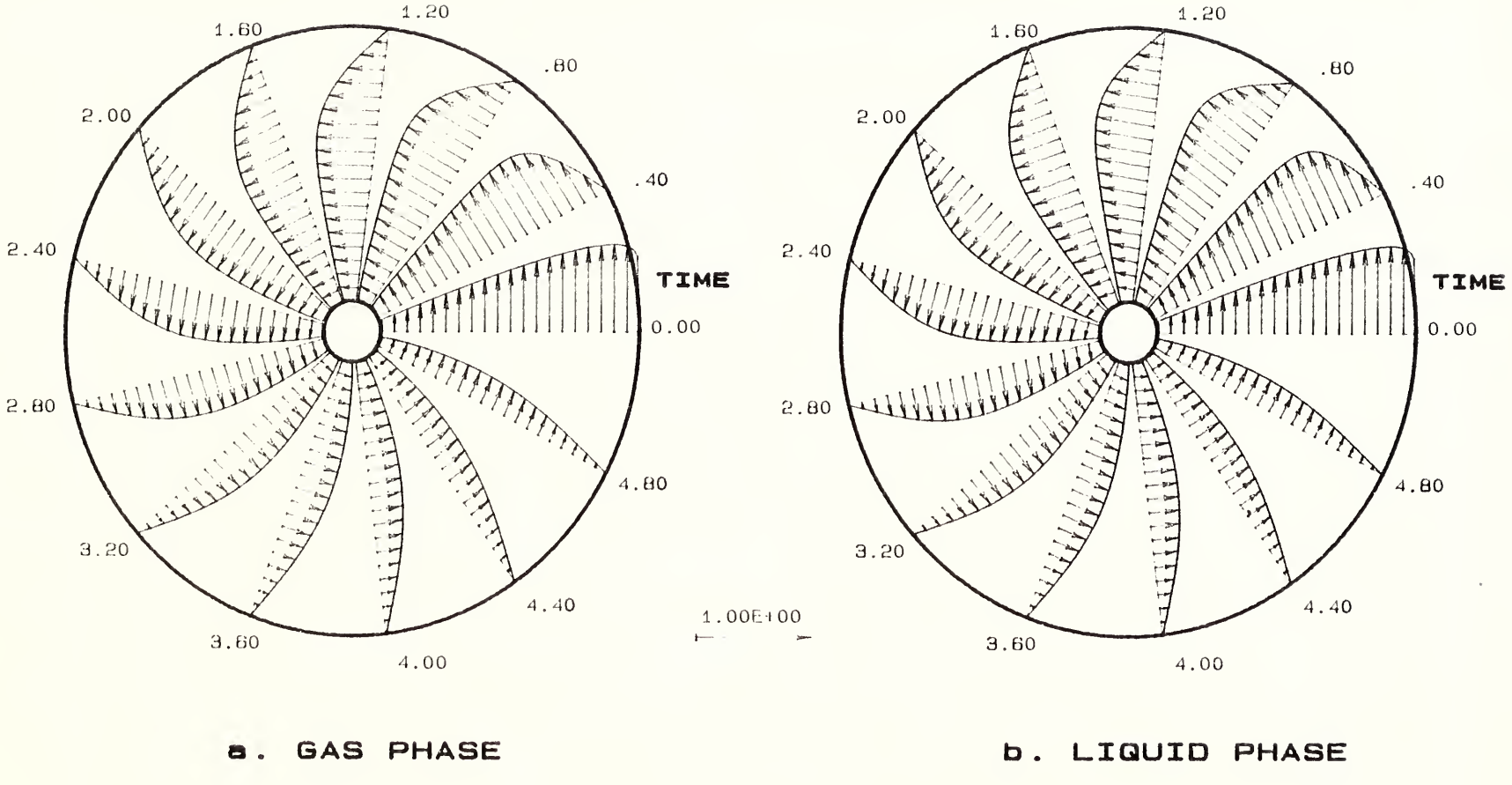

Figure 11. Velocity Vector Distributions of Test #148

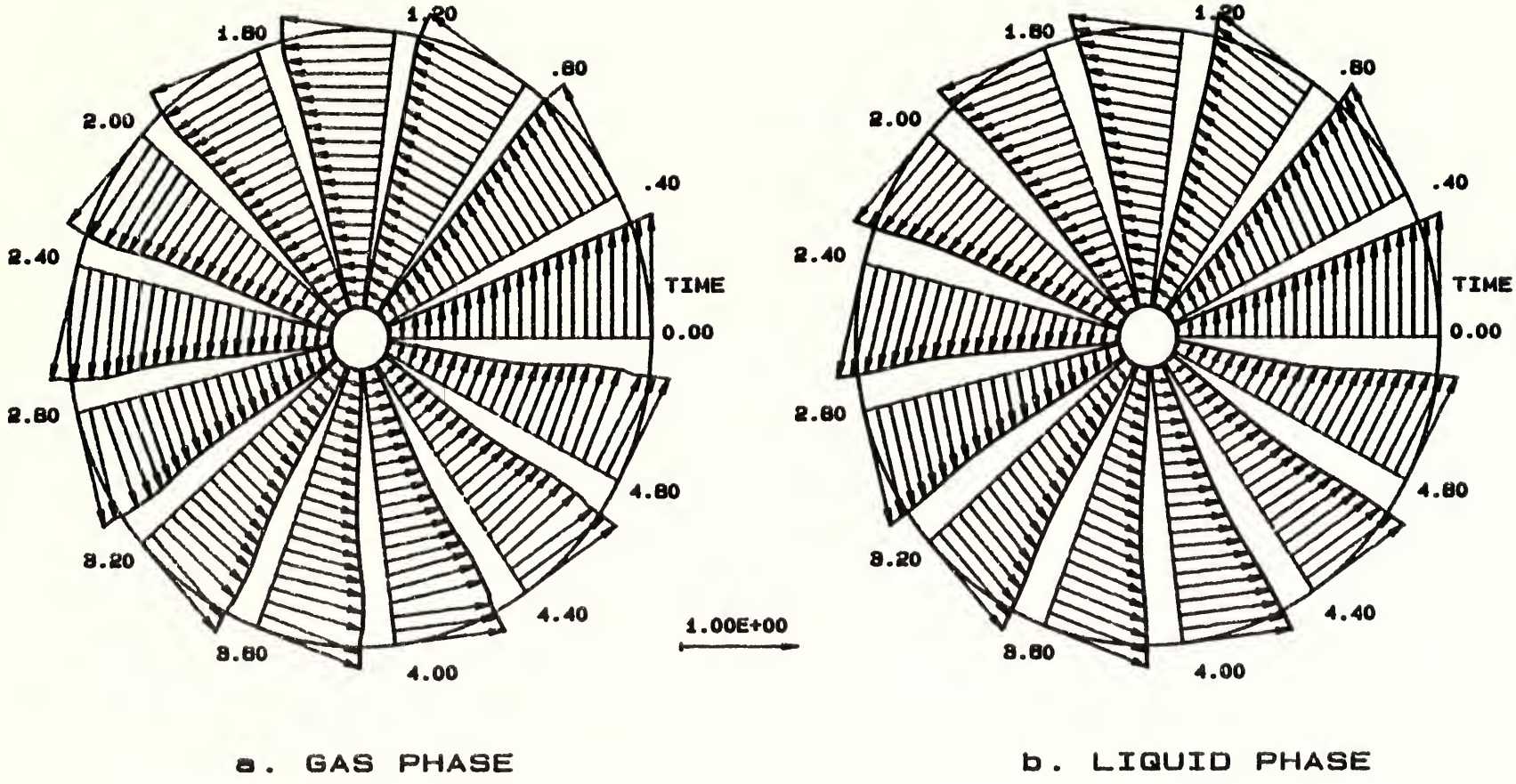

Figure 12. Velocity Vector Distributions for Test Run #150

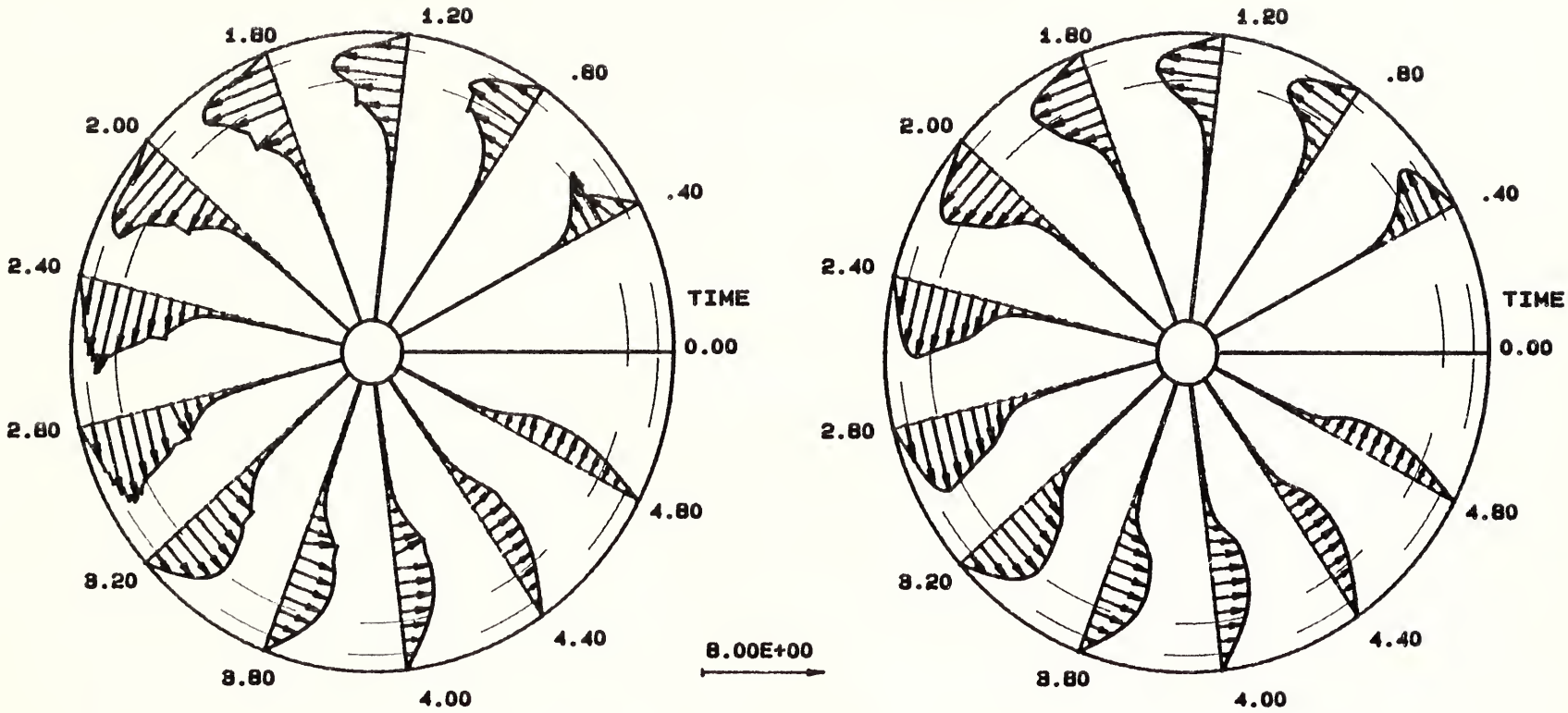

Figure 13. Velocity Vector Distributions of Test Run #151
The annular region between two dashed circles is the region of injection.

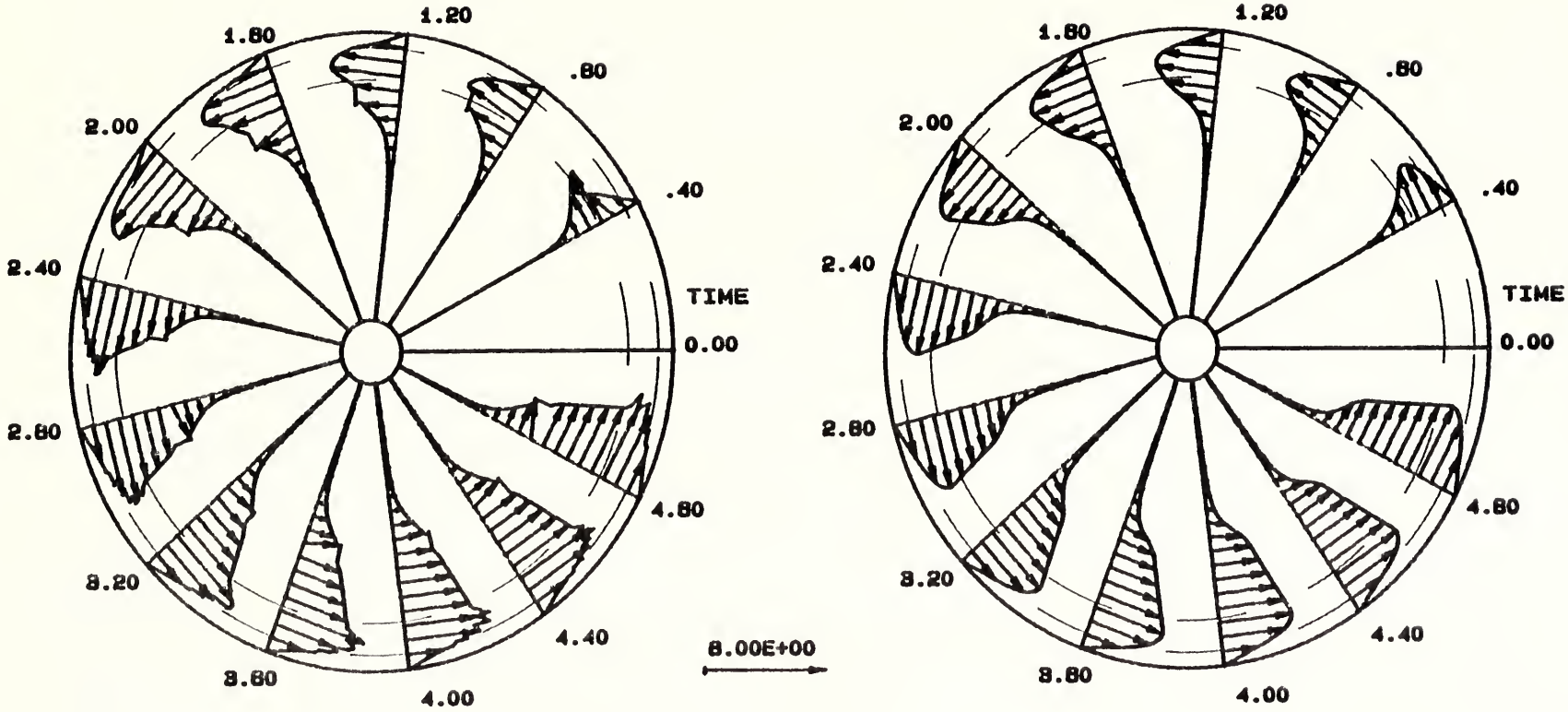

Figure 14. Velocity Vector Distributions of Test Run #152
The annular region between two dashed circles is the region of injection.

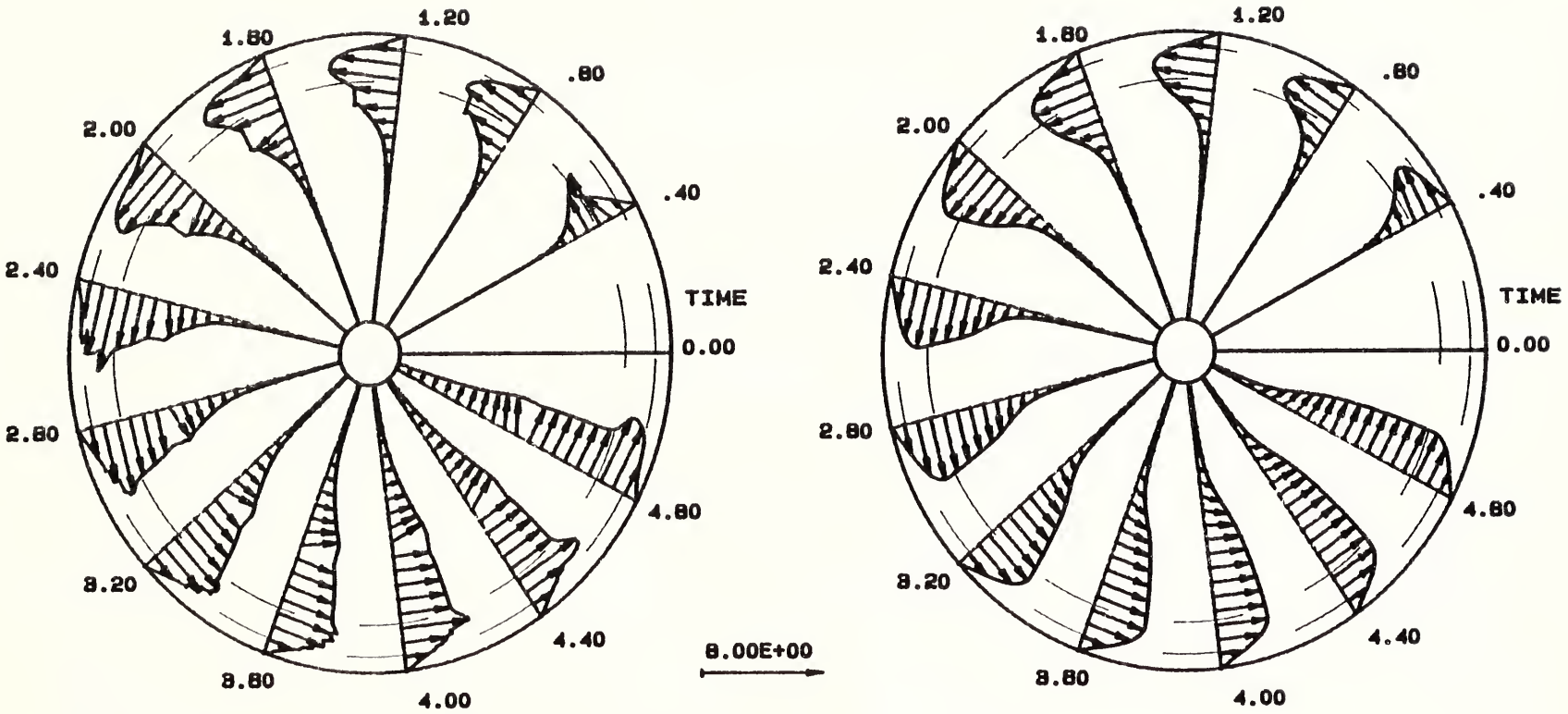

Figure 15. Velocity Vector Distributions of Test Run #153
The annular region between two dashed circles is the region of injection.

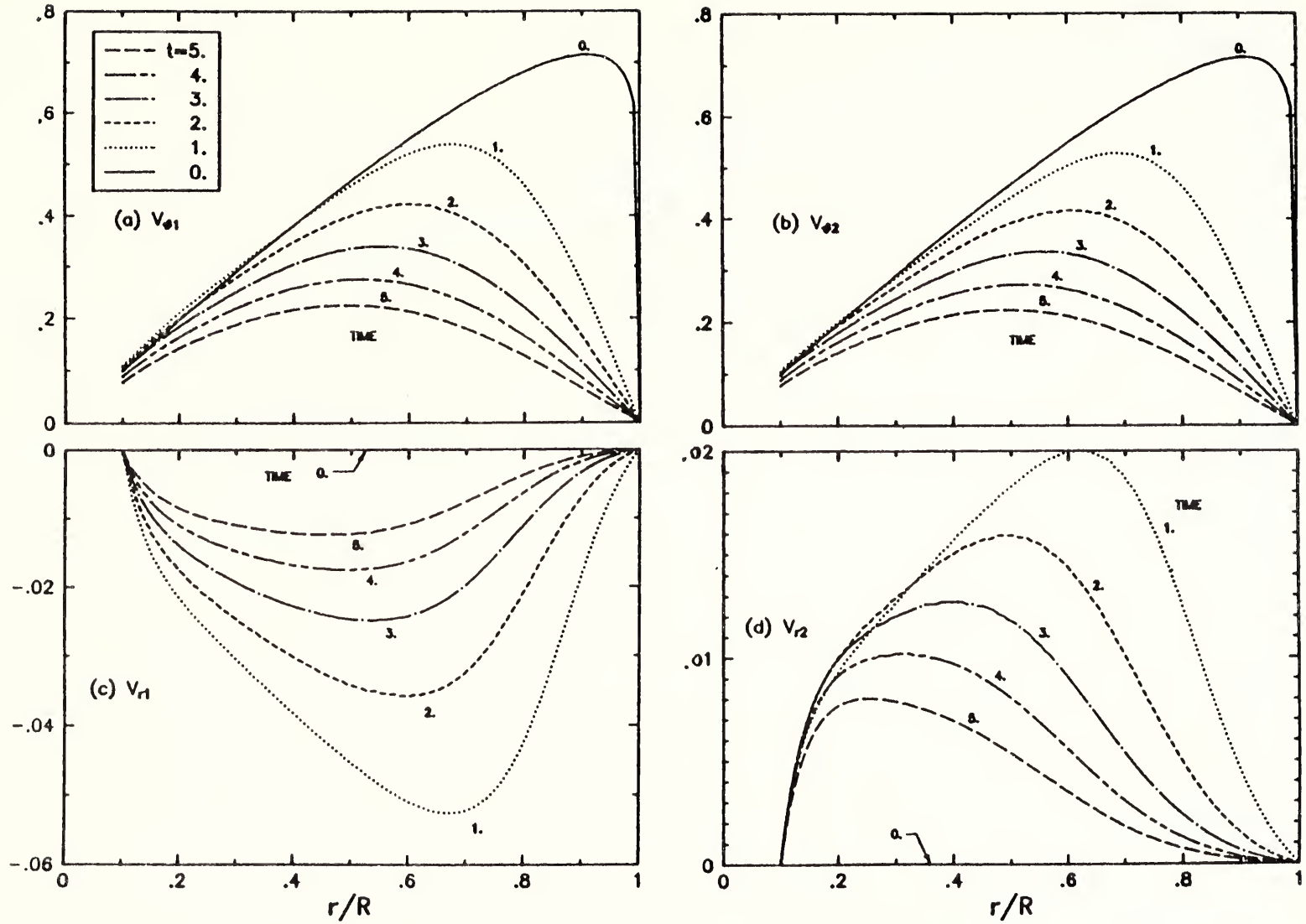

Figure 16. Velocity Distributions of Test #148
a) Gas tangential velocity, b) Liquid tangential velocity, c) Gas radial velocity, d) Liquid radial

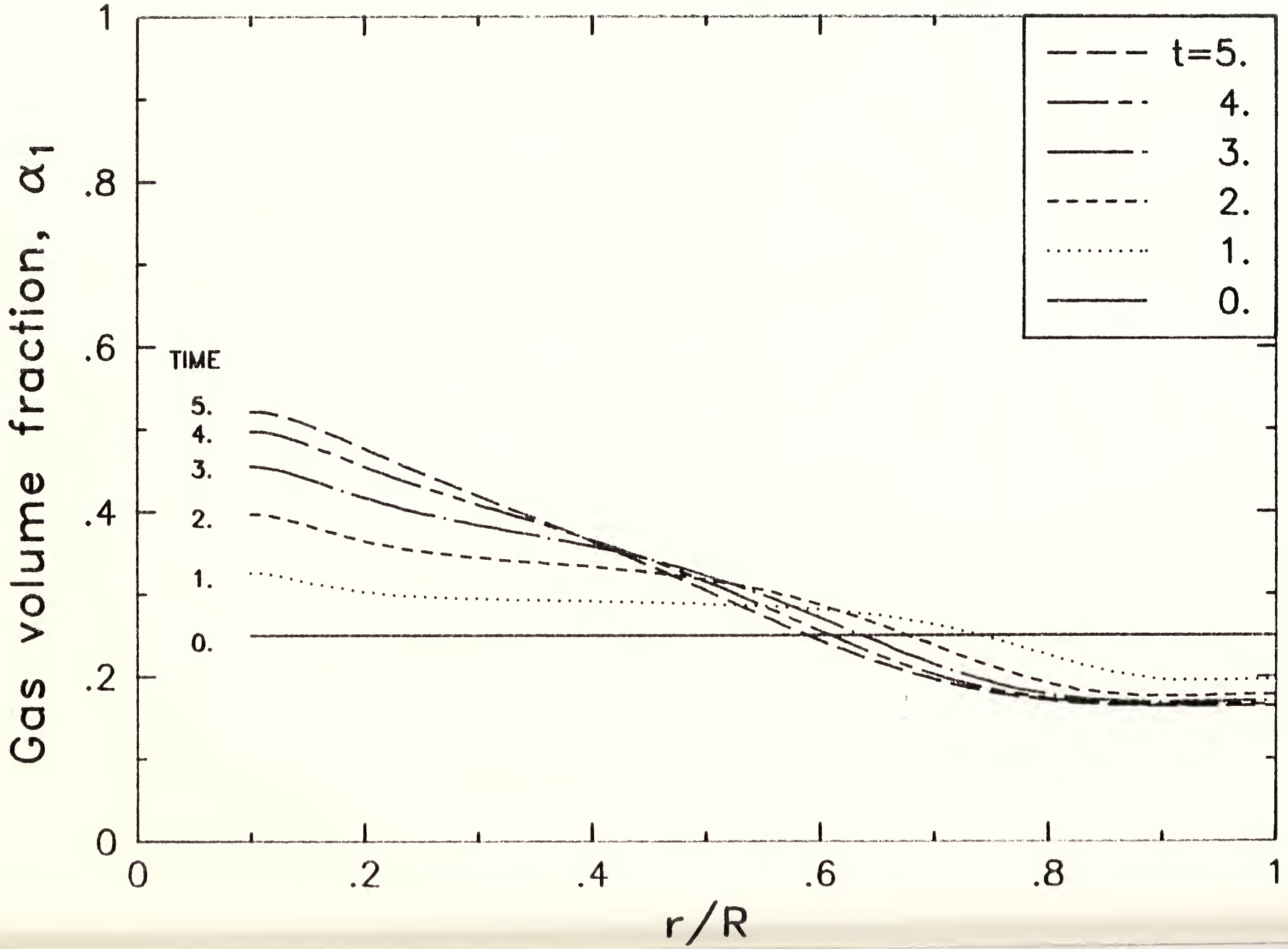
Gas volume fraction, α_1
r/R
0
.2
.4
.6
.8
1
TIME
5.
4.
3.
2.
1.
0.
t=5.
4.
3.
2.
1.
0.

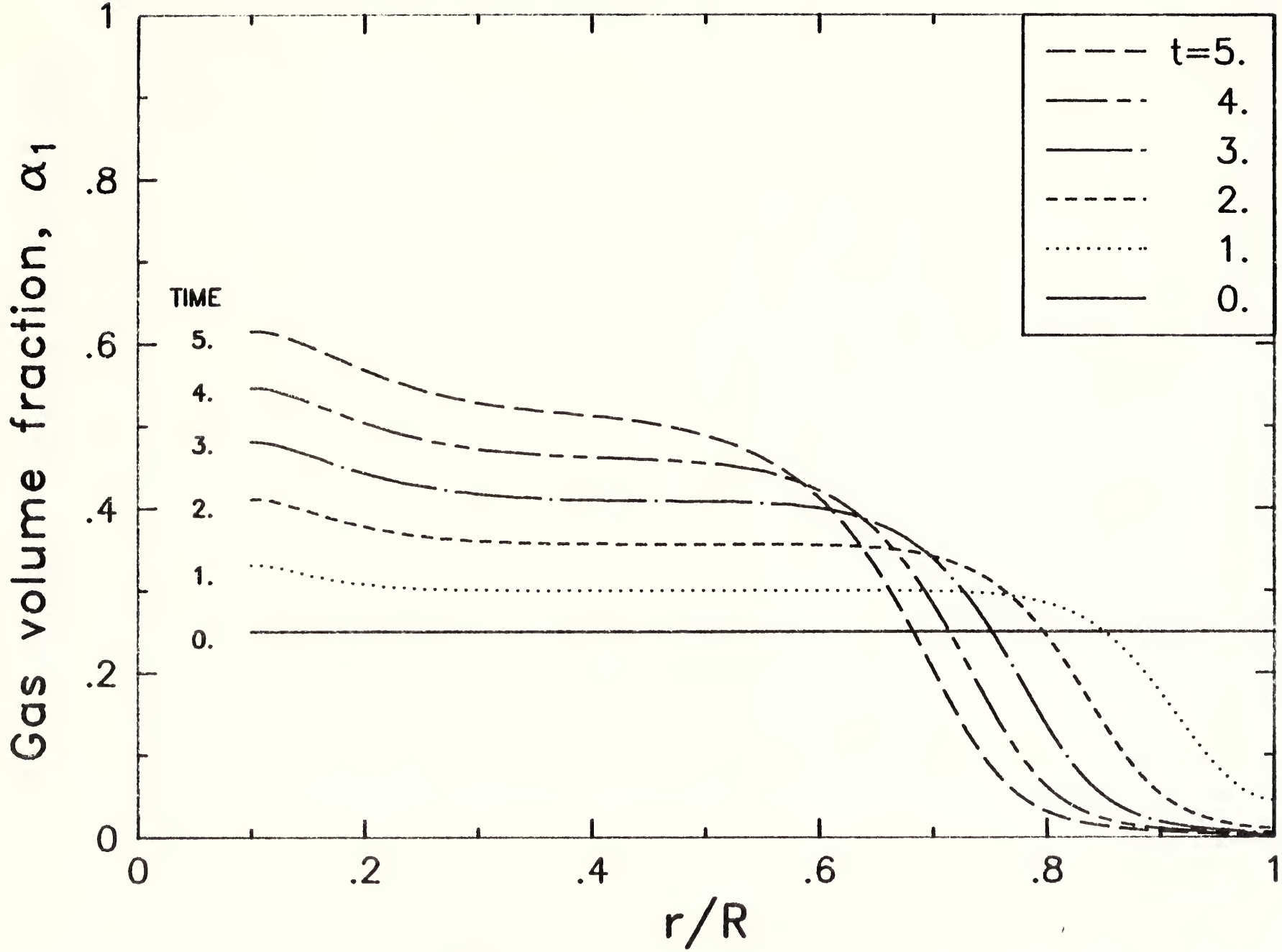

Figure 18. Gas Volume Fraction Distributions of Test #150

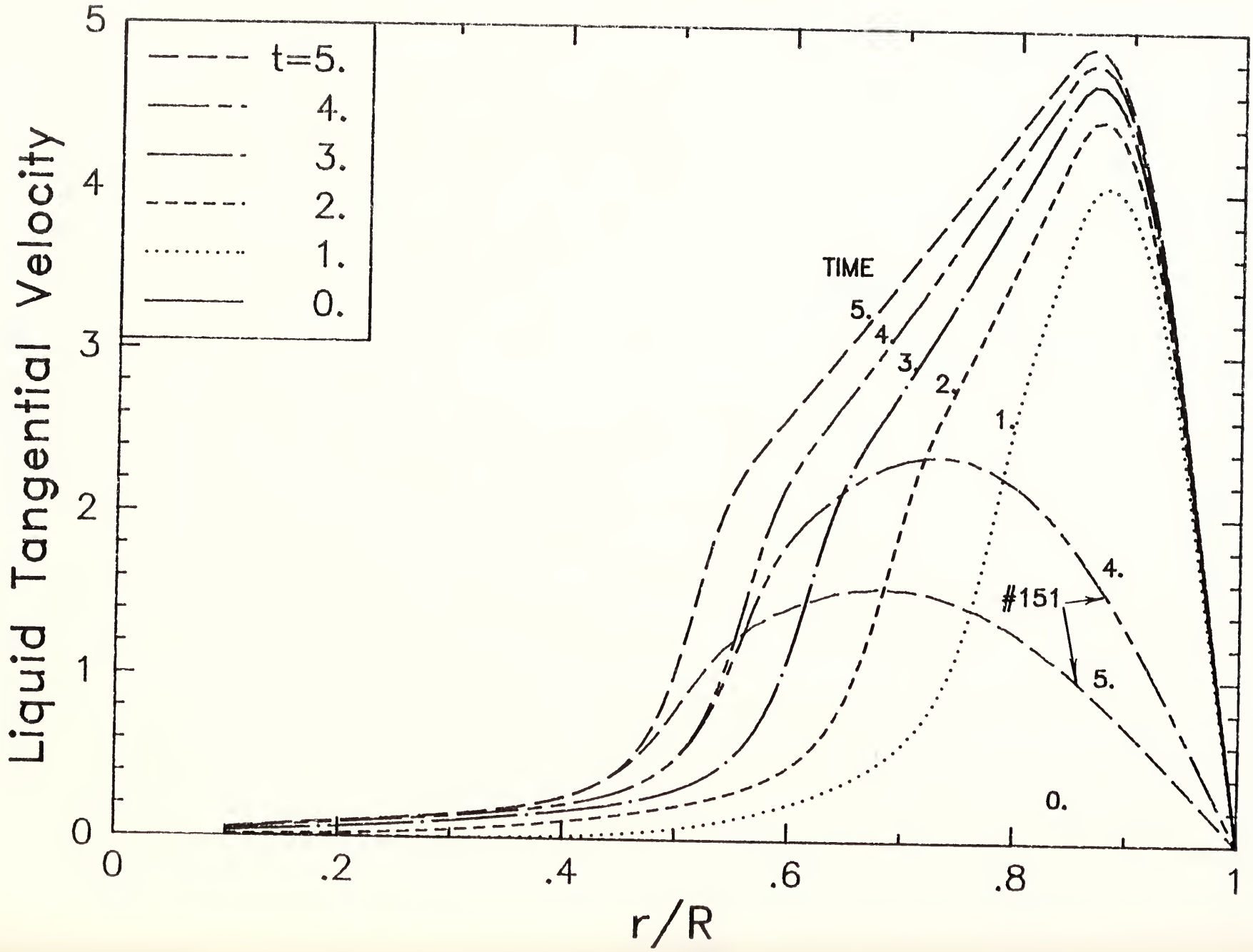

Figure 19(a). Liquid Tangential Velocity Distributions of Test #152

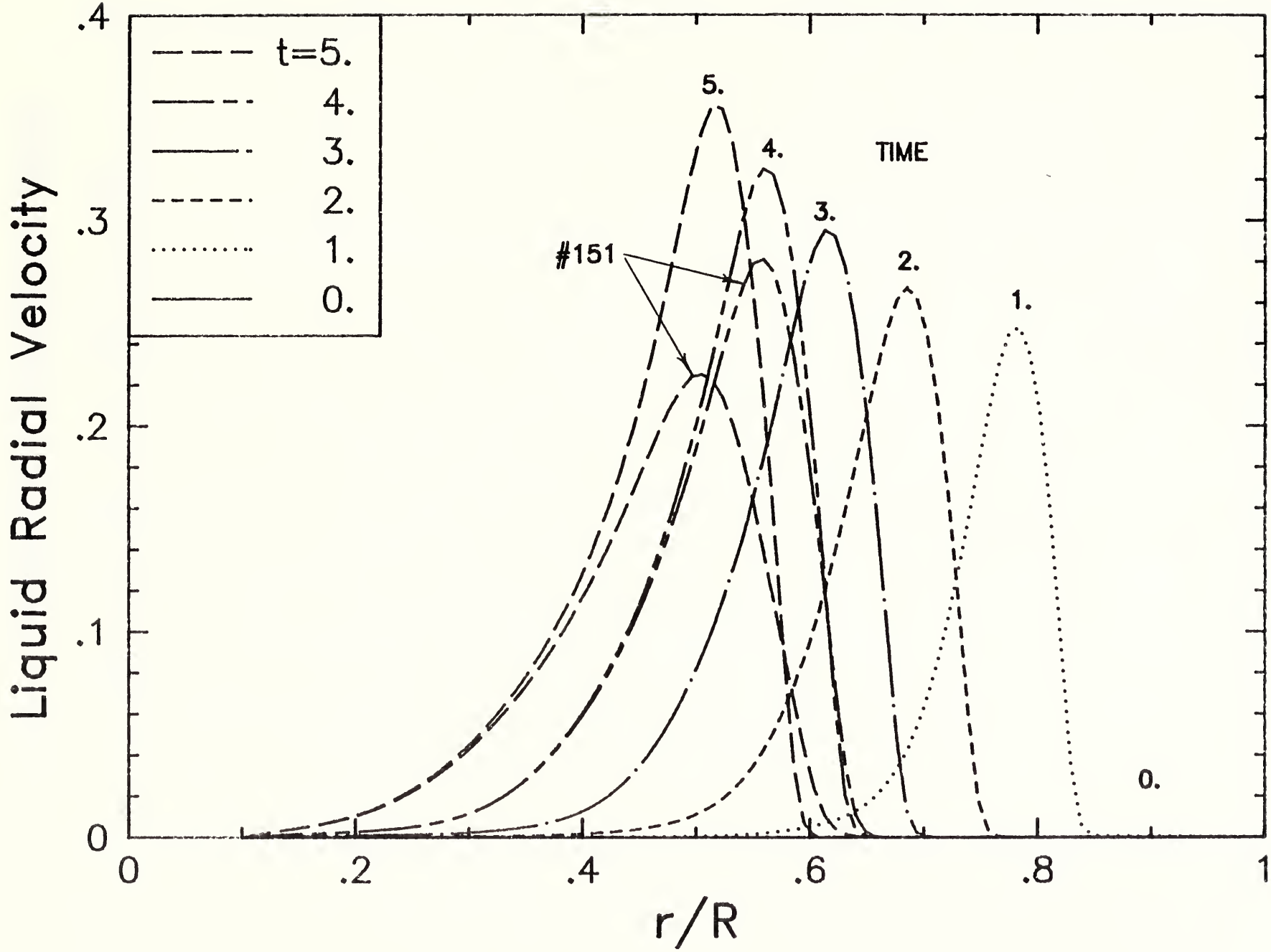

Figure 19(b). Liquid Radial Velocity Distributions of Test #152

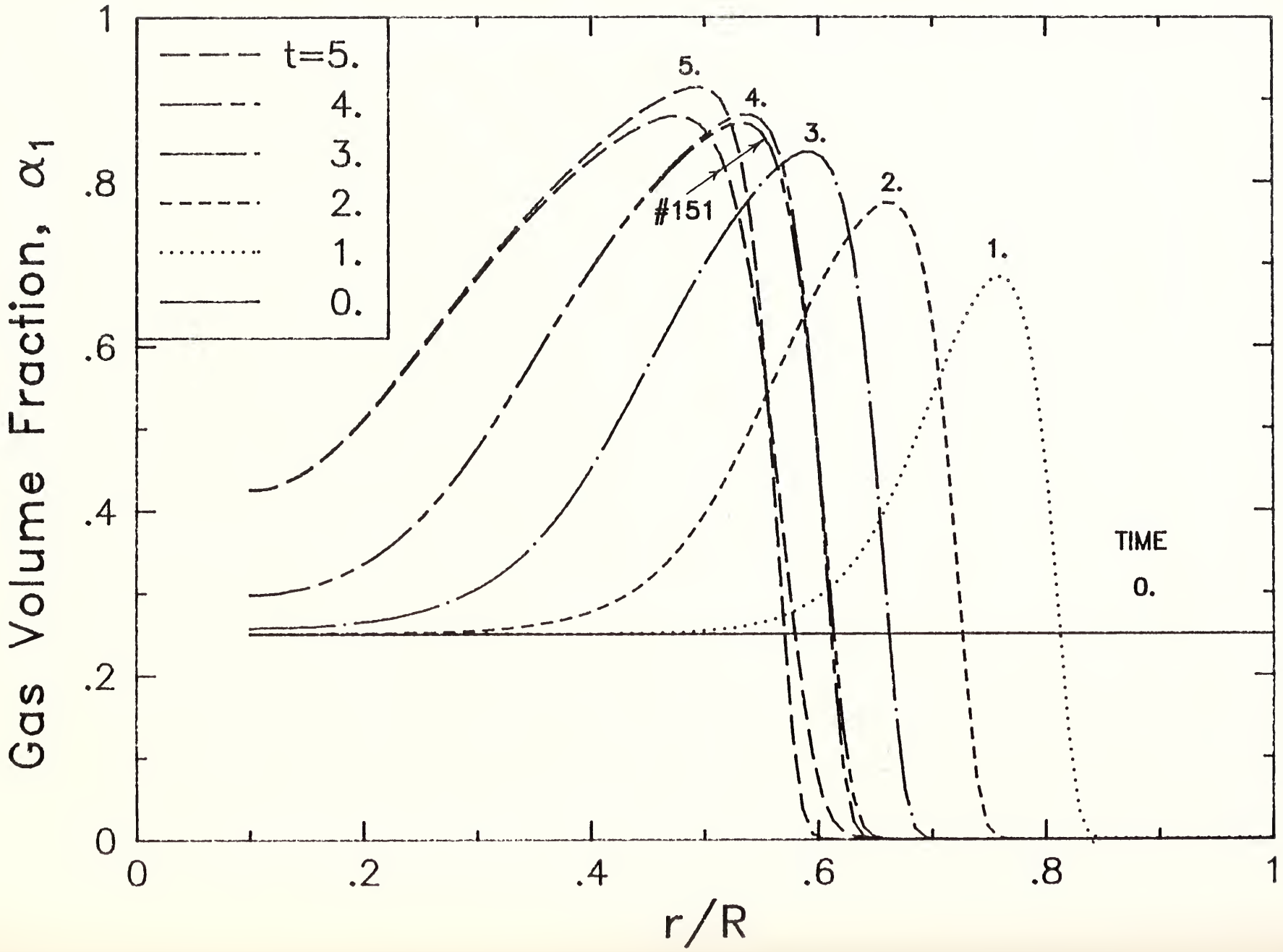

Figure 20. Gas Volume Fraction Distributions of Test #152

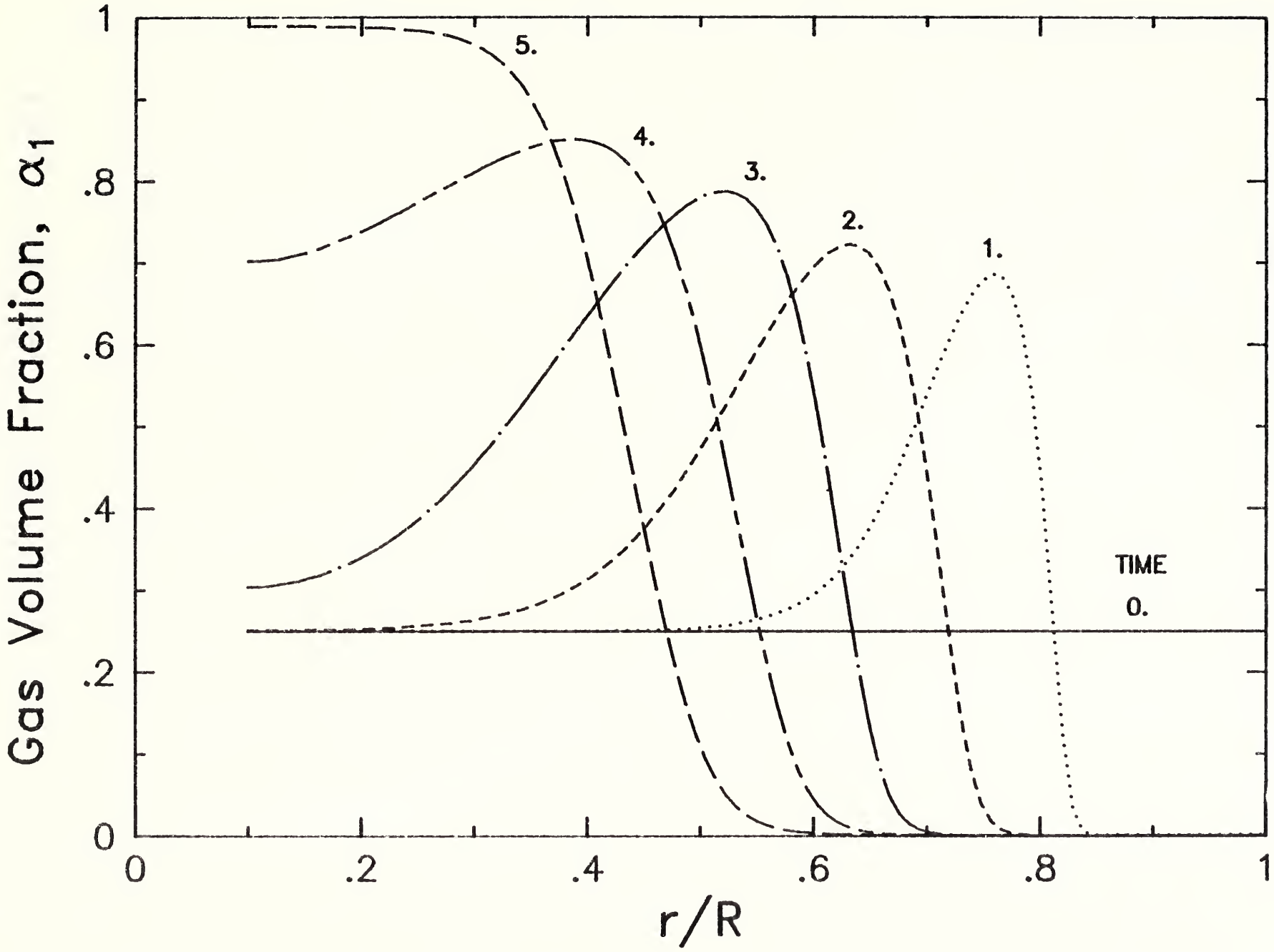

Figure 21. Gas Volume Fraction Distributions of Test #153

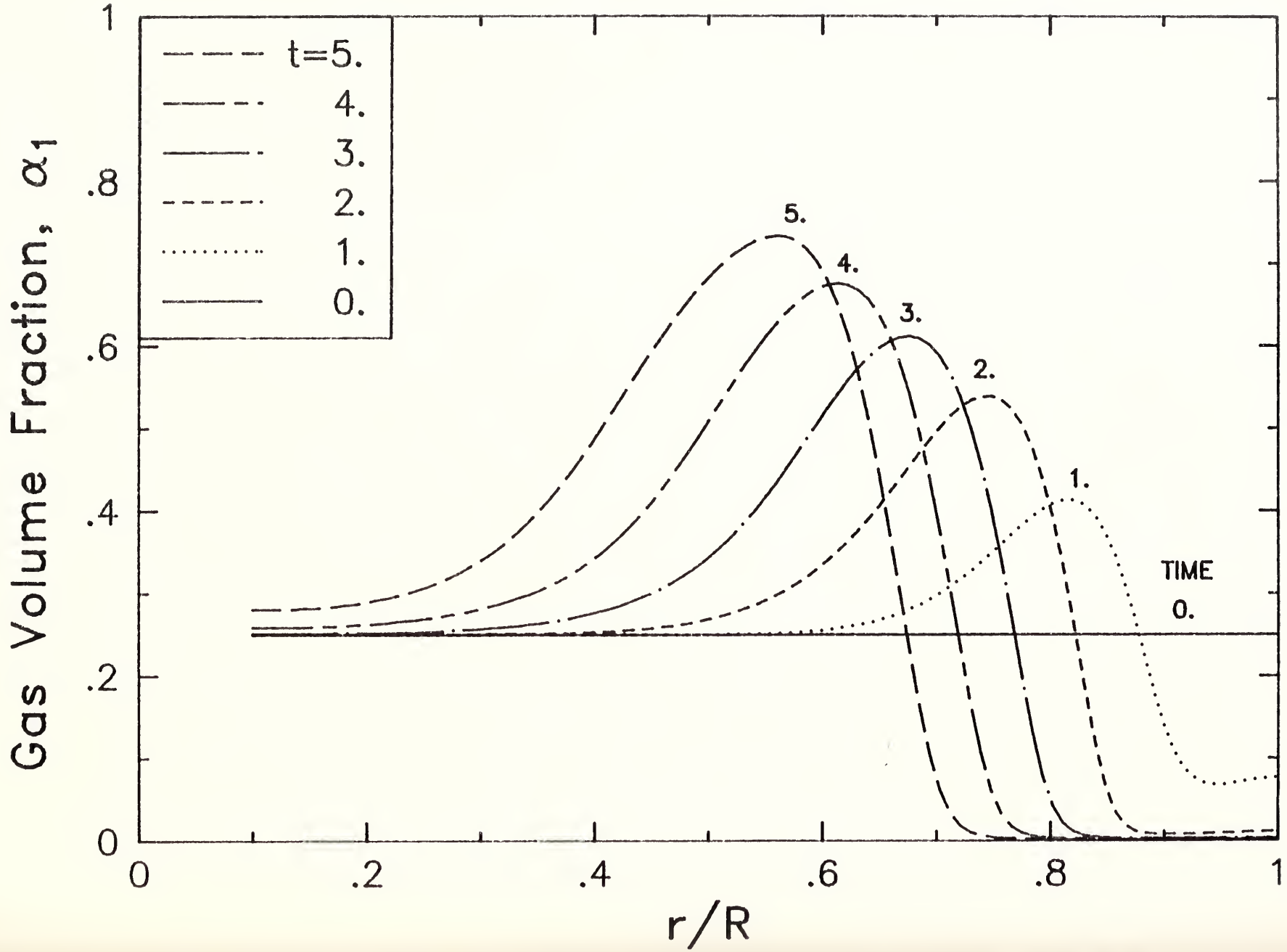

Figure 22. Gas Volume Fraction Distributions of Test #154

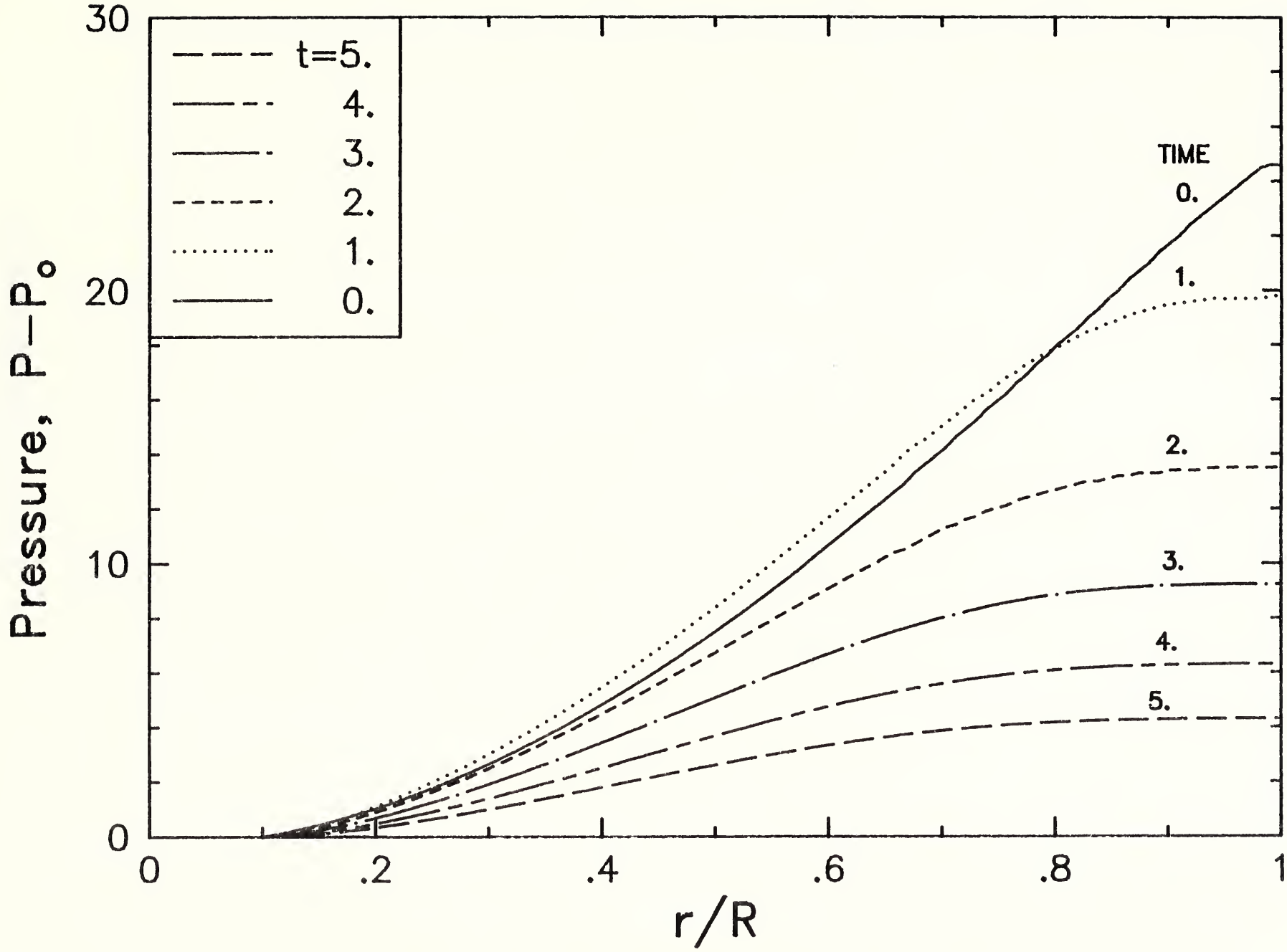

Figure 23. Pressure Distributions of Test #148

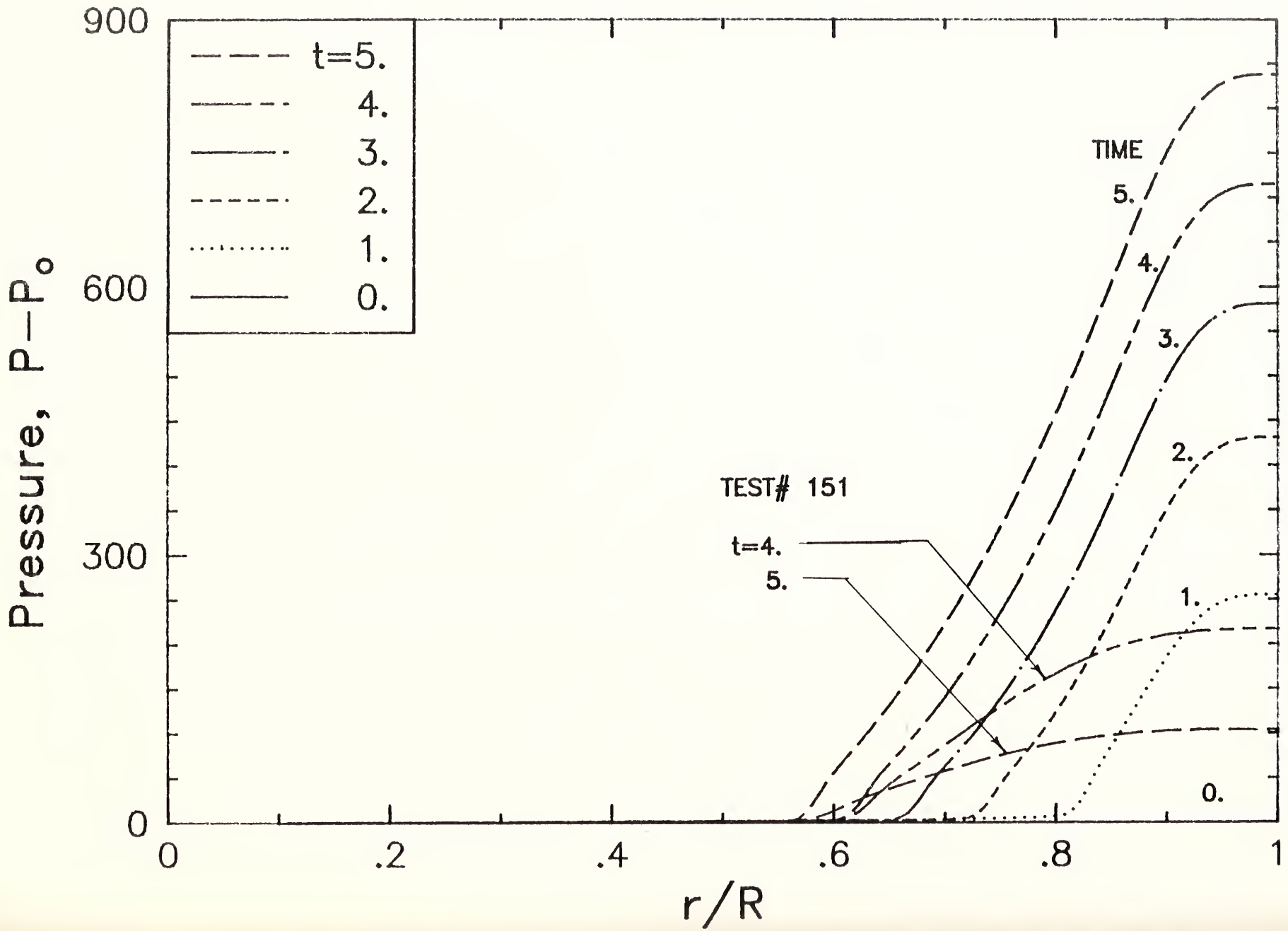

Figure 24. Pressure Distributions of Test #153

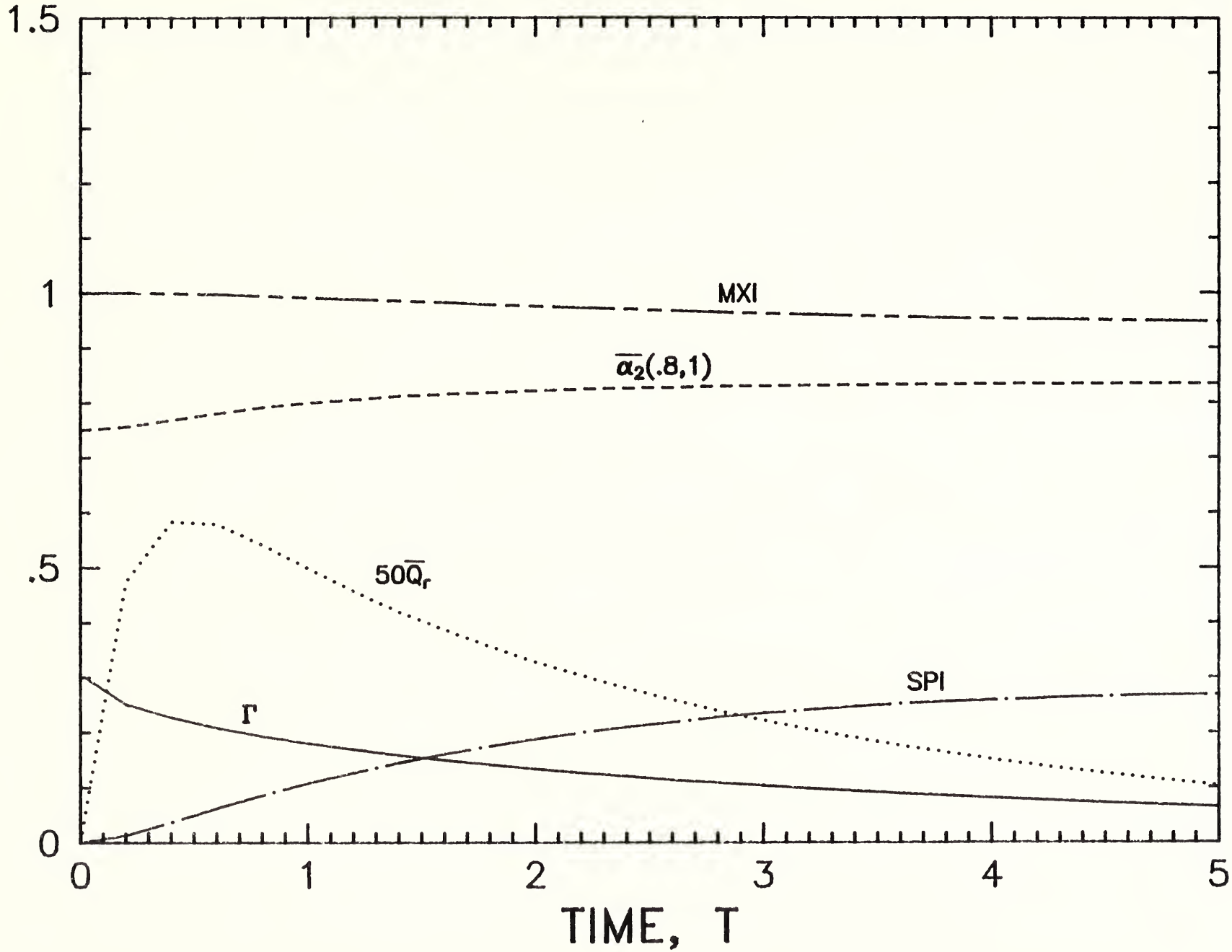

Figure 25. The Vortex Strength and Quantities on the Degree of Phase Separation of Test #148

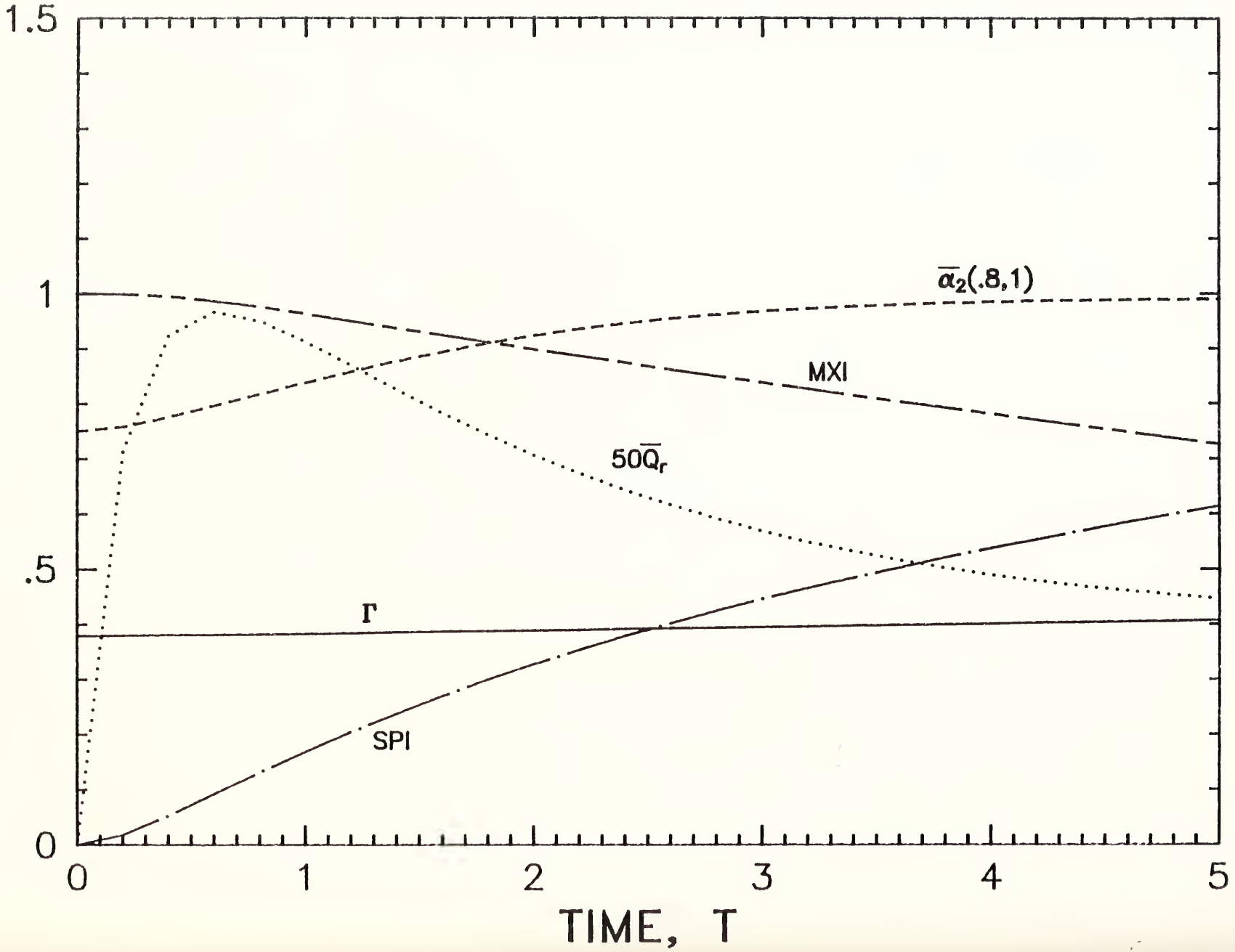

Figure 26. The Vortex Strength and Quantities on the Degree of Phase Separation of Test #150

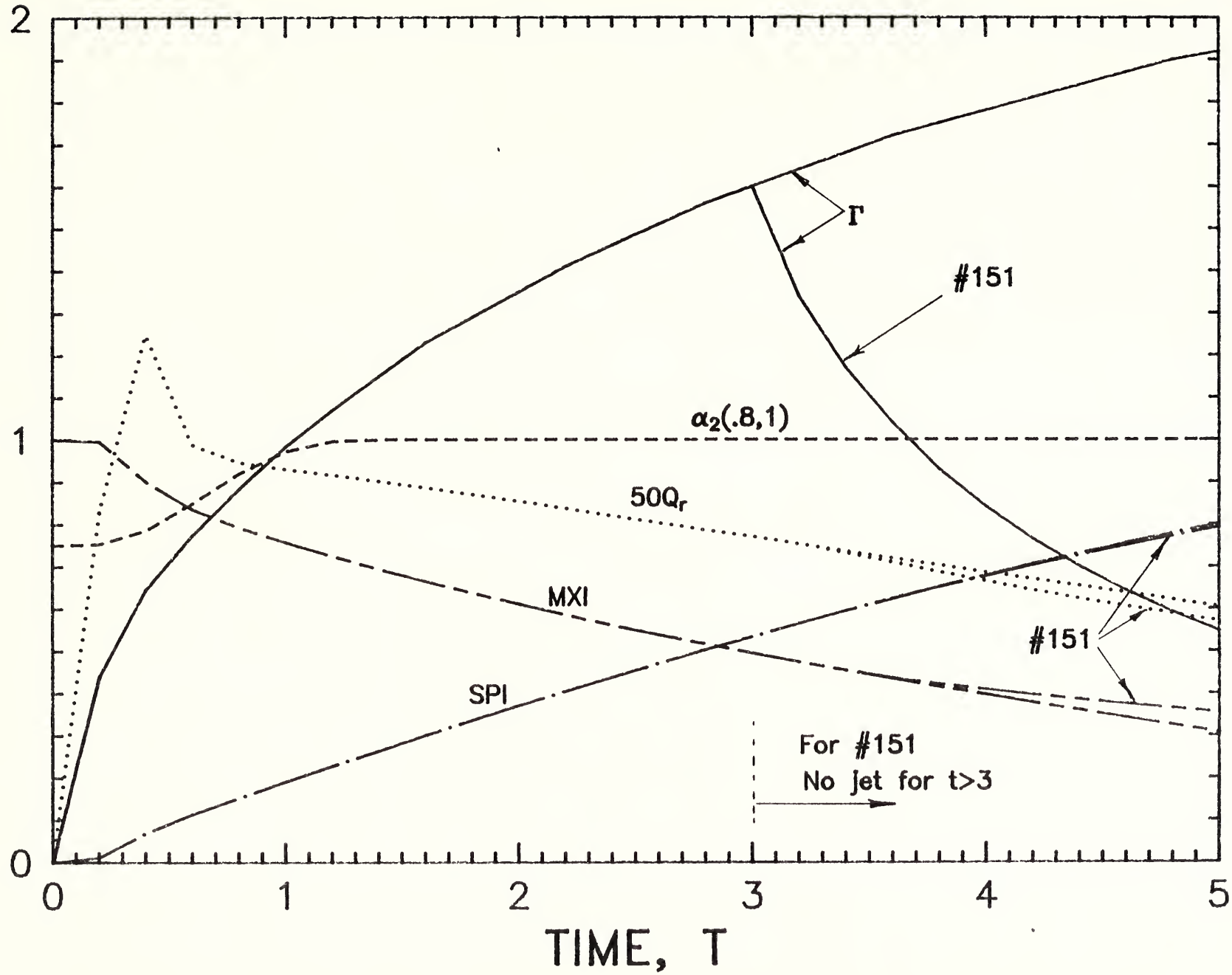

Figure 27. The Vortex Strength and Quantities on the Degree of Phase Separation of Test #152

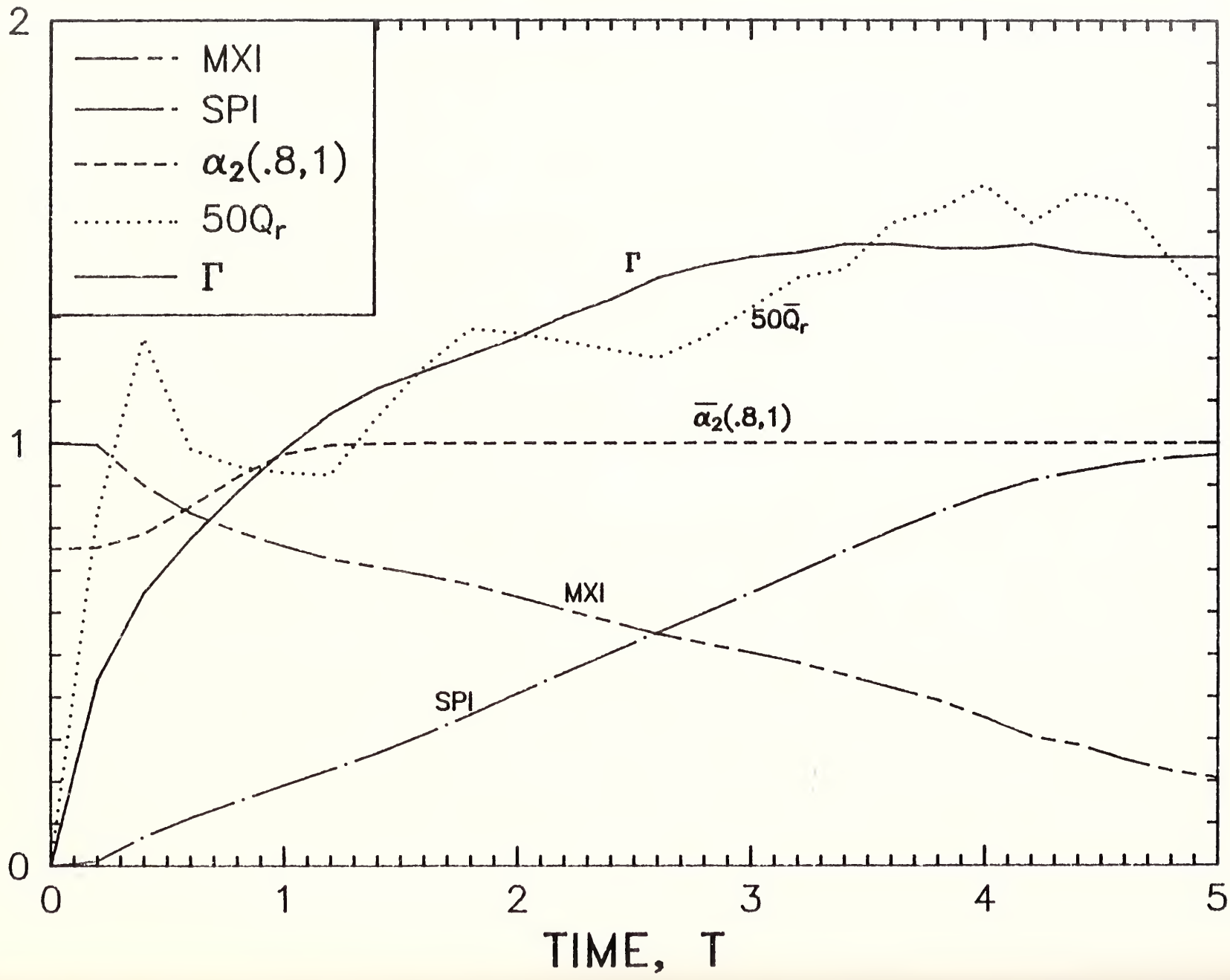

Figure 28. The Vortex Strength and Quantities on the Degree of Phase Separation of Test #153

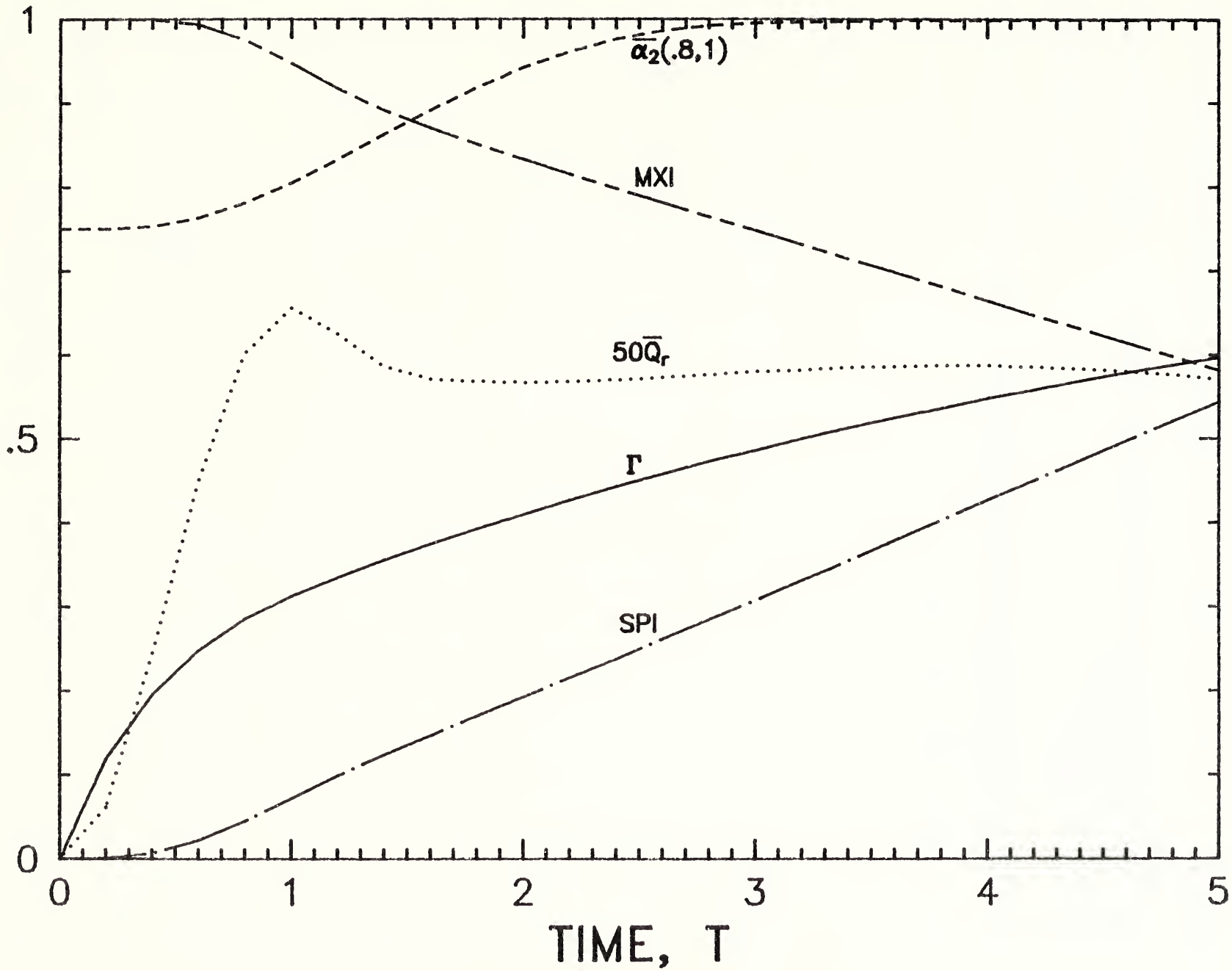

Figure 29. The Vortex Strength and Quantities on the Degree of Phase Separation of Test #154

NBS-114A (REV. 2-80)

U.S. DEPT. OF COMM. BIBLIOGRAPHIC DATA SHEET (See instructions)	1. PUBLICATION OR REPORT NO. NBSIR 86-3322	2. Performing Organ. Report No.	3. Publication Date FEBRUARY 1986

4. TITLE AND SUBTITLE

A Vortex-Induced, Gas-Liquid Separation in a Cylindrical Tank at Zero Gravity

5. AUTHOR(S)

T. T. Yeh

6. PERFORMING ORGANIZATION (If joint or other than NBS, see instructions)

NATIONAL BUREAU OF STANDARDS
DEPARTMENT OF COMMERCE
WASHINGTON, D.C. 20234

7. Contract/Grant No.

8. Type of Report & Period Covered

Final

9. SPONSORING ORGANIZATION NAME AND COMPLETE ADDRESS (Street, City, State, ZIP)

National Aeronautics and Space Administration
John F. Kennedy Space Center
Kennedy Space Center, FL 32899

10. SUPPLEMENTARY NOTES

☐ Document describes a computer program; SF-185, FIPS Software Summary, is attached.

11. ABSTRACT (A 200-word or less factual summary of most significant information. If document includes a significant bibliography or literature survey, mention it here)

The absence of body force and natural orientation of the liquid and gas in space is a major difference between the fuel transfer in space and that on earth. A vortex-induced, liquid handling process adapted to two-phase fluids in zero gravity has been analyzed for a selected range of fluid and flow parameters. This transfer process has been divided in two stages: the initial "spin-up" stage and the liquid pumped down stage. The initial spin-up stage is established by the tangential fluid injection. The model is based on a two-phase, two-fluid continuum with several phase interactions - namely fluid drag and pertinent virtual mass.

A computer program was developed to study the fluid dynamical behavior of two-phase fluids in the sender tank. Several examples are given to demonstrate the products of the program. The interested and plausible results indicate the simplified two-phase two-fluid model is a useful model. However, a detailed evaluation of the result is only possible with the aid of accurate local measurements. These verifications should be devised to check both the formulations selected for phase interactions as well as the results predicted.

12. KEY WORDS (Six to twelve entries; alphabetical order; capitalize only proper names; and separate key words by semicolons)

fuel transfer in zero gravity, gas-liquid separation; numerical modeling; rotational flows; two-phase flows, vortex motions; vortex-induced phase separations

13. AVAILABILITY

☒ Unlimited

☐ For Official Distribution. Do Not Release to NTIS

☐ Order From Superintendent of Documents, U.S. Government Printing Office, Washington, D.C. 20402.

☒ Order From National Technical Information Service (NTIS), Springfield, VA. 22161

14. NO. OF PRINTED PAGES

97

15. Price

$9.95